A gain scheduled robust linear quadratic regulator for vehicle direct yaw moment control

WANG, Zhengyuan, MONTANARO, Umberto, FALLAH, Saber, SORNIOTTI, Aldo and LENZO, Basilio <http://orcid.org/0000-0002-8520-7953>

Published version

WANG, Zhengyuan, MONTANARO, Umberto, FALLAH, Saber, SORNIOTTI, Aldo and LENZO, Basilio (2018). A gain scheduled robust linear quadratic regulator for vehicle direct yaw moment control. Mechatronics, 51, 31-45.

Vehicle Yaw Moment Control Using a Gain Scheduling Robust Linear Quadratic Regulator

Zhengyuan Wang, Umberto Montanaro, Saber Fallah, Aldo Sorniotti, Basilio Lenzo

***Abstract*—Yaw moment control systems improve vehicle stability and handling in severe driving manoeuvres. Nevertheless, the control system performance is limited by the unmodelled dynamics and parameter uncertainties. To guarantee robustness of the control system against system uncertainties, this paper proposes a gain scheduling Robust Linear Quadratic Regulator (RLQR), in which an extra control term is added to the feedback of a conventional LQR to limit the closed-loop tracking error in a neighbourhood of the origin of its state-space, despite of the uncertainties and persistent disturbances acting on the plant. In addition, the intrinsic parameter-varying nature of the vehicle dynamics model with respect to the longitudinal vehicle velocity can jeopardize the closed-loop performance of fixed-gain control algorithms in different driving conditions. Therefore, the control gains optimally vary based on the actual longitudinal vehicle velocity to adapt the closed-loop system to the variations of this parameter. The effectiveness of the proposed RLQR in improving the robustness of classical LQR against model uncertainties and parameter variations is proven analytically, numerically and experimentally. The numerical and experimental results are consistent with the analytical analysis proving that the proposed RLQR reduces the ultimate bound of error dynamics.**

I. Introduction

Modern vehicle safety control systems are critical to the enhancement of lateral vehicle stability and the reduction of fatal accidents. Safety control systems based on direct yaw moment control (DYC) enhance vehicle stability during cornering. In such systems, the yaw moment adjustment is obtained from the difference of traction/braking forces between the left and right wheels. A DYC can be actuated through the friction brakes, mechanical differentials, or individually controlled electric motors. The implementation of DYC through the friction brakes is not desirable, as it causes vehicle velocity reduction, and consequently degrades driving comfort. On the other hand, mechanical differentials are characterized by significant mechanical complexity and actuation delays. However, DYC actuation through individually controlled motors is less complex and more effective, because of the precise torque controllability of electric machines [1]–[4].

Typically, a DYC system adopts a hierarchical control structure, consisting of three separate control layers, namely the high-level controller, the mid-level controller, and the low-level controller. The high-level controller is responsible for the reference

The first two authors, Zhengyuan Wang and Umberto Montanaro, equally contributed to this research.
This work was supported by the European Union Seventh Framework Programme FP7/2007-2013 under the iCOMPOSE project under Grant 608897.
Z.Wang, U.Montanaro, S.Fallah, and A.Sorniotti are with the Centre for Automotive Engineering, University of Surrey, Guildford, GU2 7XH, U.K. (e-mail: zhengyuan.wang@surrey.ac.uk; u.montanaro@surrey.ac.uk; s.fallah@surrey.ac.uk a.sorniotti@surrey.ac.uk). B. Lenzo was with the Centre for Automotive Engineering, University of Surrey, Guildford, GU2 7XH, U.K. He is now with the Department of Engineering and Mathematics, Sheffield Hallam University, Sheffield, S1 1WB, U.K. (e-mail: basilio.lenzo@shu.ac.uk).
Corresponding Author: Umberto Montanaro (u.montanaro@surrey.ac.uk)

generation and usually outputs the reference yaw moment for the mid-level controller which distributes the reference yaw moment signals to the available actuators (e.g. electric motors, friction brakes, etc.). The low-level controller is responsible for the actuation of each actuator based on the distributed signals by mid-level controller [5].

For high-level controller, different control techniques, such as model predictive control [6], [7], robust control [8]–[10] and sliding mode control [11], [12], have been proposed in the technical literature. However, Linear Quadratic Regulators (LQR) is one of the most commonly used control method for reference yaw moment generation. To enhance tracking performance for a wide range of longitudinal velocities, the solution of the Jacobi-Riccati equation of the LQR optimisation was exploited by Refs. [13]–[15] to formulate variable feedback and feedforward gains as functions of vehicle longitudinal velocity. However, closed-loop stability of the resulting control systems were not systematically investigated for time varying longitudinal velocities, and represent a concern for such methods. Furthermore, LQR algorithms suffer from a limited gain margin against parameter perturbation and external disturbances [16], [17]. The robustness of LQR methods depend on the selection of the weights in the cost function to be minimized which also affect the closed-loop response [16]. Usually, such weights are the result of time-consuming trial and error numerical procedures aiming to find a satisfactory trade-off between robustness and performance [18]. Alternatively, to increase system robustness against disturbances and uncertainties without increasing the complexity of the design, LQR methods have been augmented with Variable Structure Control (VSC) actions. For example, a robust optimal sliding-mode yaw rate controller was proposed in [15] to address the tracking problem under uncertain conditions. A sliding mode controller with time-varying sliding surfaces to solve the optimal control problem for both linear and nonlinear systems was presented in Ref. [19]. Furthermore, a LQR/VSC method based on the Planes Cluster Approaching Mode (PCAM) to guarantee global asymptotic stability in the presence of parameter perturbation and unmodelled dynamics was developed in [20]. However, despite their theoretical effectiveness to suppress bounded disturbances, discontinuous control terms, typically embedded in sliding mode control solutions, induce chattering on the control action. In automotive applications, chattering may results either in stress and wear of mechanical or electrical parts, with a consequence damage of the system in short time, or vibrations during implementation [21]. In addition, when the discontinuous control action is smoothed to mitigate chattering, often it is not possible to prove the asymptotic convergence to zero of the tracking error but only its boundedness [21].

Considering the abovementioned challenges, this paper proposes a novel approach to improve robustness of LQR against model uncertainties, real-time system parameter variations, and disturbances for DYC applications, which allows to confine the tracking error in a pre-assigned neighbourhood of the origin despite the time-varying nature of the longitudinal velocity and without adding discontinuous actions. More specifically, the proposed control action consists of three terms, i.e., (i) a feedback action whose gain is derived by solving the algebraic Riccati equation; (ii) a feedforward action based on the reference trajectory; and (iii) a feedback robust control action to improve closed-loop robustness to unmodelled dynamics and parameter uncertainties. The all control gains

are a function of the longitudinal velocity to optimally tune the gains for wider range of speeds. Therefore, the controller belongs to the class of gain scheduling Robust Linear Quadratic Regulator (RLQR). It is noted that, the proposed RLQR method also allows the decoupled design of the LQR control action and the robust action, thus avoiding the use of time-consuming tuning for the selection of the LQ weights. The LQ weights can be chosen without considering model imperfects and disturbances. Then, based on the Riccati solution, the robust term can be designed to suppress uncertainties. The closed-loop tracking error dynamics are analytically proven to be globally uniformly ultimately bounded and an upper-bound for the ultimate bound (i.e., the maximum residual error when time goes to infinity [22]) is formulated, where, the proof is carried out by considering the plant dynamics as a parameter-varying system [23]. Hence, unwanted dynamics, which can be induced by gain scheduling strategies [24], cannot emerge. In addition, the ultimate bound is inversely proportional to the gain of the robust action, confirming the advantage provided by the proposed feedback control action. For the numerical validation, the novel RLQR is embedded in IPG CarMaker in which a prototype electric Range Rover Evoque is modelled. A quantitative comparison clearly shows that the novel RLQR outperforms gain-scheduling LQR control solutions proposed by [13], in terms of residual tracking error, peak yaw rate error and absolute value of the control action. Finally, experimental results on the same prototype electric Range Rover Evoque with individually controlled motors on front and rear axles confirm the applicability and the effectiveness of the proposed control strategy to real scenarios. Furthermore, an additional detailed comparative analysis, carried out with experimental data, points out that superior close-loop tracking performance can be achieved when the RLQR replaces gain-scheduling LQRs available in the literature [13].

The rest of the paper is organized as follow. Section II describes the vehicle models for control system design and reference generation. Section III focuses on the control problem definition and control law formulation, while Section IV is dedicated to the analysis of the closed-loop tracking error dynamics by using a Lyapunov approach. The numerical analysis for different relevant manoeuvres is carried out in Section V by means of co-simulations, while Section VI discusses the implementation of the controller on the electric vehicle demonstrator as well as the analysis of the experimental results. Conclusions are summarised in Section VII together with possible future extensions.

II. VEHICLE SYSTEM MODELLING AND REFERENCE SIGNAL DESIGN

The first step to design control systems for vehicle lateral stability enhancement is to formulate a proper set of reference signals based on the vehicle handling and stability characteristics. To this aim, the bicycle vehicle model, shown in Figure 1, is used. Despite its simplicity, the model reproduces well the main handling and stability characteristics of a vehicle during cornering. Hence, it is often used in the technical literature at the control design stage.

Figure 1. A two-degree-of-freedom bicycle model.

By denoting as δ the steering angle, v_x and v_y the longitudinal and lateral components of vehicle velocity, respectively, and with F_{yf} and F_{yr} the lateral forces of the front and rear tyres, the equations of motion are:

$$m\left(v_x\dot{\beta} + v_x r\right) = F_{yf} + F_{yr}, \tag{1}$$

$$I_z\dot{r} = L_a F_{yf} - L_b F_{yr} + u, \tag{2}$$

where β is the vehicle sideslip angle, L_a and L_b are the front and rear semi-wheelbases, r is vehicle yaw rate, I_z is the yaw moment of inertia about the vehicle yaw axis, and m is the vehicle mass and u is the torque which is generated to turn the vehicle around the axis and it is used as the vehicle control input. It is noted that, the actuator bandwidth is often much larger than that of the closed-loop system, thus, according to the recent literature [1], [13], [15], its dynamics are neglected in the controller design.

For the system in Eqs. (1) and (2) a linear approximation of the lateral forces has been adopted, thus F_{yf} and F_{yr} are expressed in accordance with [13], [14] as:

$$F_{yf} = C_{\alpha f}\alpha_f, \tag{3}$$

$$F_{yr} = C_{\alpha r}\alpha_r, \tag{4}$$

where $C_{\alpha f}$ and $C_{\alpha r}$ are the cornering stiffness of the front and rear axles, respectively, while α_f and α_r represent the slip angles of front and rear axles, respectively. Moreover, α_f and α_r can be computed as:

$$\alpha_f = \delta - \beta - tan^{-1}\frac{L_a r}{v_x} \approx \delta - \beta - \frac{L_a r}{v_x}, \tag{5}$$

$$\alpha_r = -\beta + tan^{-1}\frac{L_b r}{v_x} \approx -\beta + \frac{L_b r}{v_x}, \tag{6}$$

where the approximation in Eqs. (5) and (6) have been obtained by assuming small slip angles. Considering Eqs. (1) to (6), the state-space formulation of the vehicle model can be expressed as:

$$\dot{x} = Ax + Bu + E\delta, \tag{7}$$

where u is the control yaw moment, $x = [\beta \quad r]^T$ is the system state, while the system matrices are:

$$A = \begin{bmatrix} -\frac{C_{\alpha r} + C_{\alpha f}}{m v_x} & \frac{C_{\alpha r} L_b - C_{\alpha f} L_a}{m v_x^2} - 1 \\ \frac{L_b C_{\alpha r} - L_a C_{\alpha f}}{I_z} & -\frac{{L_b}^2 C_{\alpha r} + {L_a}^2 C_{\alpha f}}{I_z v_x} \end{bmatrix}, \quad B = \begin{bmatrix} 0 \\ \frac{1}{I_z} \end{bmatrix}, \quad E = \begin{bmatrix} \frac{C_{\alpha f}}{m v_x} \\ \frac{L_a C_{\alpha f}}{I_z} \end{bmatrix}. \tag{8}$$

The reference yaw rate is calculated as the yaw rate of the passive bicycle model in steady-state conditions which provides consistently linear reference vehicle behaviour. After algebraic manipulations, the steady-state yaw rate, r_{ss}, is:

$$r_{ss} = \frac{v_x}{L(1 + k_{us} {v_x}^2)} \delta, \tag{9}$$

where L is the wheelbase and k_{us} is the understeering gradient or stability factor [5]:

$$k_{us} = \frac{m\left(L_a C_{\alpha f} - L_b C_{\alpha r}\right)}{L^2 C_{\alpha f} C_{\alpha r}}. \tag{10}$$

Equation (9) shows that in steady-state conditions the yaw rate is a linear function of the steering angle. However, in practice the maximum achievable yaw rate is limited by the tyre-road friction coefficient. By imposing steady-state cornering conditions and re-arranging Eq. (1), the maximum absolute value of the reference yaw rate is given by $\frac{\mu g}{v_x}$ [1], where μ is the tyre-road friction coefficient and g is the gravity. Considering this bound, the steady-state reference yaw rate, r_b, is:

$$r_b = min\left\{|r_{ss}|, c\frac{\mu g}{v_x}\right\} sgn(\delta), \tag{11}$$

where c is a constant coefficient that can be used as a safety factor [13]. In practice, significant inaccuracy in the μ-estimation can occur and therefore a value of $c < 1$ ensures that the reference yaw rate is within the achievable limits. Usually, the value of the parameter c is chosen as a trade-off between cornering performance and safety. The value of the parameter c is chosen in the range of 0.8 to 0.95 which provides a satisfactory cornering performance without being too conservative. Hence, the absolute value of r_b coincides with the smaller value between $|r_{ss}|$ and $c\frac{\mu g}{v_x}$. The sign of the steering angle, i.e., $sgn(\delta)$, is introduced in Eq. (11) to obtain the correct direction of the reference yaw rate. Since the reference signal (11) may not be smooth, a modified yaw rate reference, denoted as r_{ref}, is considered by applying a first order lag filter to r_b [13].

$$r_{ref} = \frac{1,}{1 + \tau_r s} r_b, \tag{12}$$

with τ_r being the time constant of the filter.

In this paper, the reference sideslip angle is set to be zero to ensure vehicle stability in any condition. Alternatively, the sideslip reference can be calculated with the same method proposed for the reference yaw rate, i.e., based on the steady-state lateral response of the bicycle vehicle model.

III. PROBLEM DEFINITION AND CONTROL FORMULATION

In this section, the problem of controlling the vehicle yaw rate is reformulated as a model reference problem and a robust LQ-based algorithm is proposed to impose the reference dynamics to system (7) despite possible parameter uncertainties and disturbances. As previously mentioned, the resulting control action is composed of three terms: (i) a feedback action, u_{LQ}, whose gain is derived by solving the algebraic Riccati equation; (ii) a feedforward action, u_{FF}, based on the reference trajectory; and (iii) an extra feedback term, u_{RB}, to improve closed-loop robustness to disturbances.

The main parameter uncertainty in system (7) is the tyre cornering stiffness. In general, the variations of cornering stiffness are caused by tyre nonlinearities with slip angle, camber angle and vertical load [26]. To consider such uncertainties, the front and rear cornering stiffness are modelled as

$$C_{\alpha f} = C_{\alpha f_0} + \Delta C_{\alpha f}, \tag{13}$$

$$C_{\alpha r} = C_{\alpha r_0} + \Delta C_{\alpha r}, \tag{14}$$

with $C_{\alpha f_0}$and $C_{\alpha r_0}$ being the nominal front and rear cornering stiffness values, respectively, while $\Delta C_{\alpha f}$ and $\Delta C_{\alpha r}$ represent the uncertain terms, which are bounded. Consequently, system (7) can be rewritten as:

$$\dot{x} = (A_0(v_x) + \Delta A)x + Bu + (E_0 + \Delta E)\delta \tag{15}$$

where A_0 and E_0 are the nominal matrices of the system, with $A_0(v_x)$ being defined as

$$A_0(v_x) = \begin{bmatrix} -\dfrac{C_{\alpha r_0} + C_{\alpha f_0}}{m v_x} & \dfrac{C_{\alpha r_0} L_b - C_{\alpha f_0} L_a}{m v_x^2} - 1 \\ \dfrac{L_b C_{\alpha r_0} - L_a C_{\alpha f_0}}{I_z} & -\dfrac{L_b^2 C_{\alpha r_0} + L_a^2 C_{\alpha f_0}}{I_z v_x} \end{bmatrix}, \tag{16}$$

where $\Delta A = A - A_0$ and $\Delta E = E - E_0$ are the parameter uncertainties.

Notice that the dynamic matrix A_0 and E_0 depend on the longitudinal velocity v_x where such dependency makes the plant model a parameter varying system [23].

The control objective is to impose the reference trajectories, $x_d(t) = [\beta_{ref}(t),\ r_{ref}(t)]^T$, with $\beta_{ref}(t) = 0$, to the state of system (15). The reference dynamics are:

$$\dot{x}_d = A_d x_d + E_d \delta, \tag{17}$$

where the system matrices are

$$A_d = \begin{bmatrix} 0 & 0 \\ 0 & -\dfrac{1}{\tau_r} \end{bmatrix}, \quad E_d = \begin{bmatrix} 0 \\ \dfrac{G}{\tau_r} \end{bmatrix}, \tag{18}$$

with $G = min\left\{\left|\frac{v_x}{L(1+k_{us}v_x^2)}\right|, c\frac{\mu g}{v_x|\delta|}\right\}$.

In this paper, the model reference control problem is solved by selecting u as

$$u(t; v_x) = u_{FF}(t; v_x) + u_{LQ}(t; v_x) + u_{RB}(t; v_x), \tag{19}$$

where

$$u_{FF}(t; v_x) = -I_z\left[\frac{1}{\tau_r}r_{ref} - \frac{L_b^2 C_{\alpha r_0} + L_a^2 C_{\alpha f_0}}{I_z v_x}r_{ref} - \left(\frac{G}{\tau_r} - \frac{L_a C_{\alpha f_0}}{I_z}\right)\delta\right], \tag{20}$$

$$u_{LQ}(t; v_x) = K_{LQ}(v_x)e(t) = R^{-1}B^T P(v_x)e(t), \tag{21}$$

$$u_{RB}(t; v_x) = \bar{K}_{RB}(v_x)e(t) = k_{RB}B^T P(v_x)e(t), \tag{22}$$

where $e(t)$ is the tracking error defined as $e(t) = x_d(t) - x(t)$, $R \in \mathbb{R}$ and $k_{RB} \in \mathbb{R}$ are positive constants, and $P(v_x) \in \mathbb{R}^{2\times 2}$ is the solution of the algebraic Riccati equation

$$A_0^T(v_x)P(v_x) + P(v_x)A_0(v_x) + Q - P(v_x)BR^{-1}B^T P(v_x) = 0, \tag{23}$$

which is solved as function of the longitudinal vehicle speed $v_x \in [v_{xmin}, v_{xmax}]$, with v_{xmin} and v_{xmax} being the minimum and the maximum longitudinal velocities of the vehicle, respectively, and $Q \in \mathbb{R}^{2\times 2}$ is a symmetric strictly positive definite matrix. Besides, it is assumed that there exists $\varepsilon_p \in (0, 1)$ such that the following condition holds

$$-(1-\varepsilon_p)Q - PBR^{-1}B^T P + \frac{\partial P}{\partial v_x}a_x \leq 0\,, \;\; \forall\, a_x \in [a_{xmin}, a_{xmax}], \tag{24}$$

where a_x is the longitudinal vehicle acceleration and a_{xmin} and a_{xmax} are the minimum and maximum possible longitudinal accelerations such that (24) is verified.

Figure 2 shows a schematic representation of the control action (19)-(23) together with the velocity based gain scheduling mechanism for the online tuning of the control gains (i.e. $K_{LQ}(v_x)$ and $\bar{K}_{RB}(v_x)$) and the plant (i.e. the vehicle and the low level controllers for imposing the required control yaw moment [5]).

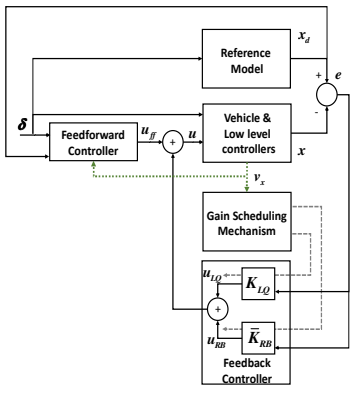

Figure 2. Robust Linear Quadratic Regulator control scheme.

Remarks

1) As indicated in Eqs. (20), (21) and (22), the control gains (K_{LQ} and $\overline{K}_{RB}$) are chosen as a function of the longitudinal velocity. Hence, the proposed control algorithm is a gain-scheduling strategy.
2) The feedforward control action, i.e., u_{FF} in Eq. (20), is that proposed in [13] and it is used to compensate the mismatch between the reference matrices (A_d, E_d) with respect to the nominal matrices (A_0, E_0). It is noted that, if $v_x(t)$ is known a priori (i.e. before the manoeuvre starts) for the entire manoeuvre and if the linear time varying system with dynamic matrix $A_0(v_x(t))$ and input matrix $E_0(v_x(t))$ provides desirable dynamics for the reference yaw rate (e.g. absence of overshoots and a satisfactory settling time), it can be used as reference model in Eq. (17), thus simplifying the control design as u_{FF} is set to zero.
3) The feedback control action u_{LQ} is the solution of the optimal LQ-problem with constant longitudinal vehicle speed and infinite control horizon [16], when the cost function to be minimized is

$$J = \frac{1}{2}\int_{t_0}^{\infty} [e^T Q e + u^T R u] dt. \tag{25}$$

4) Since, the matrix $-\big(1-\varepsilon_p\big)Q - PBR^{-1}B^T P$ is strictly negative, it is not restrictive to assume that there exists a range of longitudinal accelerations so that the term $\frac{\partial P}{\partial v_x} a_x$ which is generated by the time-varying nature of the parameter v_x, does not make the left-hand side of (24) positive.
5) As shown in the next section, the control gain k_{RB} in (22) is used to confine the closed-loop tracking error within a neighbourhood of the origin when the time goes to infinity. Specifically, it is proven that the closed-loop system is globally uniformly ultimately bounded and the ultimate bound is inversely proportional to the root-square of k_{RB}. Furthermore, it is shown that the design of k_{RB} to provide a given ultimate bound can be carried out systematically and for any a priory choose of the LQ weights, i.e. matrices Q and R in (25).

IV. Analysis of the Closed-Loop System Dynamics

This section studies the closed-loop error dynamics resulted from applying control action (19) into system (15). Due to existence of persistent disturbances acting on the closed-loop plant, the convergence to zero of the tracking error cannot be always assured. Hence, the focus of this paper is to compute an upper bound of the tracking error. Specifically, in the following, we prove that if the control input u is chosen as in Eq. (19) , then the tracking error, $e \triangleq x_d - x$, is globally uniformly ultimately bounded [22], i.e., there exists a time interval T (dependent on $e(t_0)$) and a KL-class function $\Psi: \mathbb{R}^+ \times \mathbb{R}^+ \to \mathbb{R}^+$ such that

$$\|e(t)\| \leq \Psi(\|e(t_0)\|, t - t_0) \quad \forall\, t \in [t_0, t_0 + T), \tag{26}$$

and

$$\|e(t)\| \leq \rho \quad \forall\, t \in [\, t_0 + T, +\infty). \tag{27}$$

The positive constant ρ is the ultimate bound for the closed-loop error dynamics, and it is computed as

$$\rho = \sqrt{\frac{\lambda_2}{\lambda_1(1-\varepsilon_\phi)\varepsilon_p \lambda_{min}(Q)}}\frac{d_{max}}{\sqrt{k_{RB}}}, \tag{28}$$

where

$$\lambda_1 = \inf_{v_x \in [v_{xmin},\, v_{xmax}]}\{\lambda_{min}(P(v_x))\} \quad \text{and} \quad \lambda_2 = \sup_{v_x \in [v_{xmin},\, v_{xmax}]}\{\lambda_{max}(P(v_x))\}, \tag{29}$$

with $\lambda_{min}(\Upsilon)$ and $\lambda_{max}(\Upsilon)$ being the minimum and the maximum eigenvalues of a generic positive definite matrix Υ, respectively, while ε_ϕ is a constant chosen in the open interval $(0, 1)$, and $d_{max} \in \mathbb{R}^+$ is an upper bound of the norm of the disturbance acting on the closed-loop dynamics.

The analytical proof of (26) and (27) is based on the following steps: *(a)* derivation of the tracking error dynamics; *(b)* selection of a Lyapunov function $V(e)$ such that $\sigma_1(||e||) \leq V(e) \leq \sigma_2(||e||)$, with $\sigma_1(\cdot)$ and $\sigma_2(\cdot)$ being K_∞ functions; and *(c)* proving that the derivative of $V(e)$ satisfies the condition $\dot{V}(e) \leq -\Phi(e) \;\; \forall\, e \in \mathbb{R}^2 : ||e|| \geq \vartheta$, where $\Phi : \mathbb{R}^2 \to \mathbb{R}^+$ is a positive function and ϑ is strictly positive constant. Then the global uniform ultimate boundedness of e follows from Theorem 1 (see Appendix A), which also allows to compute the ultimate bound as $\rho = \sigma_1^{-1}\big(\sigma_2(\vartheta)\big)$.

a) Tracking error dynamics:

Considering Eqs. (15) and (17), the closed-loop tracking error is given by

$$\dot{e} = \dot{x}_d - \dot{x} = A_0 e - Bu + (A_d - A_0)x_d + (E_d - E_0)\delta - \Delta A x - \Delta E \delta \tag{30}$$

Notice that in Eq. (30) the dependency with respect to the time and the longitudinal velocity is omitted for the sake of readability. By applying the control action (19), the feedforward control action u_{FF} compensates the mismatch on the second row between the reference matrices (A_d, E_d) with respect to the nominal matrices (A_0, E_0). Hence, the closed-loop dynamics can be rewritten as

$$\dot{e} = A_0 e + B\bar{u} + D(t) \tag{31}$$

where the equivalent control $\bar{u}$ and the disturbance D are defined as

$$\bar{u} = -u_{LQ} - u_{RB} \tag{32}$$

and

$$D(t) = B_1 B_1^T (A_d - A_0)x_d(t) + B_1 B_1^T (E_d - E_0)\delta(t) - \Delta A x(t) - \Delta E \delta(t) \;\text{ and }\; B_1^T = [1 \quad 0]. \tag{33}$$

As a technical assumption, the disturbance is assumed to be bounded such that $D(t) = Bd(t)$, with $|d(t)| < d_{max}$, where d_{max} is a known upper bound. Consequently, the closed loop system dynamics is given by

$$\dot{e} = A_0 e + B(\bar{u} + d(t)) \tag{34}$$

b) Selection of the Lyapunov Function:

As Lyapunov function for system (34), the following quadratic form is chosen

$$V(e) = e^T P(v_x) e. \tag{35}$$

where $P(v_x)$ is the solution of the Riccati equation (23).

From Eq. (35), it can be proved that

$$\sigma_1(||e||) \leq V(e) \leq \sigma_2(||e||) \tag{36}$$

with σ_1 and σ_2 being K_∞ functions defined as

$$\sigma_1(||e||) = \lambda_1 ||e||^2 \quad \text{and} \quad \sigma_2(||e||) = \lambda_2 ||e||^2 \tag{37}$$

where λ_1 and λ_2 are those given in Eq. (29).

c) Derivative of the Lyapunov Function and its upper bound:

The derivative of the Lyapunov function (35) can be computed as

$$\dot{V} = \dot{e}^T P e + e^T P \dot{e} + e^T \dot{P} e \tag{38}$$

Considering Eqs. (33) and (34), equality (38) can be rewritten as

$$\begin{aligned} \dot{V} &= e^T (A_0^T P + P A_0 - P B R^{-1} B^T P) e - e^T P B R^{-1} B^T P e + \dot{a}_x e^T \frac{\partial P}{\partial v_x} e + 2 e^T P B (-k_{RB} B^T P e + d) = \\ &= e^T (A_0^T P + P A_0 - P B R^{-1} B^T P + Q) e + e^T \left(-(1 - \varepsilon_p) Q - P B R^{-1} B^T + \frac{\partial P}{\partial v_x} a_x \right) e - \varepsilon_p e^T Q e + \\ &\quad + 2 e^T P B (-k_{RB} B^T P e + d), \end{aligned} \tag{39}$$

where the second equality has been obtained by adding and subtracting to the first equality the term $e^T Q e$, and rewriting such term as $e^T Q e - e^T Q e = e^T Q e - (1 - \varepsilon_p) Q - \varepsilon_p Q$.

By using (23) and (24), the derivative of the Lypunov function can be upper-bounded as

$$\dot{V} \leq -\varepsilon_p e^T Q e + 2 e^T P B (-k_{RB} B^T P e + d) \leq -\varepsilon_p \lambda_{min}(Q) \|e\|^2 - k_{RB} \|B^T P e\|^2 - k_{RB} \|B^T P e\|^2 + 2 e^T P B d. \tag{40}$$

Since the following quadratic expansion is valid,

$$\left(\sqrt{k_{RB}}\, e^T PB - \frac{d}{\sqrt{k_{RB}}}\right)^2 = k_{RB}\|B^T Pe\|^2 - 2e^T PBd + \frac{d^2}{k_{RB}} \tag{41}$$

It is possible to complete the square in Eq. (40) to get

$$\begin{aligned} \dot{V} \leq & -\varepsilon_p \lambda_{min}(Q)\|e\|^2 - k_{RB}\|B^T Pe\|^2 - k_{RB}\|B^T Pe\|^2 + 2e^T PBd = \\ =& -\varepsilon_p \lambda_{min}(Q)\|e\|^2 - k_{RB}\|B^T Pe\|^2 - \left(\sqrt{k_{RB}}\, e^T PB - \frac{d}{\sqrt{k_{RB}}}\right)^2 + \frac{d^2}{k_{RB}} \leq \\ \leq & -\varepsilon_p \lambda_{min}(Q)\|e\|^2 + \frac{d_{max}^2}{k_{RB}} = -\widetilde{\Phi}(e) \end{aligned} \tag{42}$$

with

$$\begin{aligned} \widetilde{\Phi}(e) &= \vartheta_1\|e\|^2 - \vartheta_2\,, \qquad \vartheta_1 = \varepsilon_p \lambda_{min}(Q), \\ \vartheta_2 &= \frac{d_{max}^2}{k_{RB}} \end{aligned} \tag{43}$$

which can be rewritten, for a generic $\varepsilon_\phi \in (0,1)$, as

$$\begin{aligned} \widetilde{\Phi}(e) &= \Phi(e) + (1-\varepsilon_\phi)\vartheta_1\|e\|^2 - \vartheta_2\,, \\ \Phi(e) &= \varepsilon_\phi \vartheta_1\|e\|^2, \end{aligned} \tag{44}$$

with $\Phi(e)$ being a positive function of e.

When $\|e\| \geq \vartheta$, with

$$\vartheta = \sqrt{\frac{\vartheta_2}{(1-\varepsilon_\phi)\vartheta_1}} = \frac{1}{\sqrt{(1-\varepsilon_\phi)\varepsilon_p \lambda_{min}(Q)}} \frac{d_{max}}{\sqrt{k_{RB}}} \tag{45}$$

then $(1-\varepsilon_\phi)\vartheta_1||e||^2 - \vartheta_2 \geq 0$, and therefore $\widetilde{\Phi}(e) \geq \Phi(e)$, or equivalently $-\widetilde{\Phi}(e) \leq -\Phi(e)$. Hence, the derivative of the Lyapunov function in (42) can be upper-bounded as,

$$\dot{V}(e) \leq -\Phi(e), \forall\, \|e\| \geq \vartheta. \tag{46}$$

As confirmed in Eqs. (36) and (46), all the hypothesis required by Theorem 1 in Appendix A are fulfilled and therefore the tracking error system is globally uniformly ultimately bounded and the ultimate bound is computed as given in Eq. (28):

$$\rho = \sigma_1^{-1}\big(\sigma_2(\vartheta)\big) = \sqrt{\frac{\lambda_2}{\lambda_1}}\,\vartheta = \sqrt{\frac{\lambda_2}{\lambda_1}}\sqrt{\frac{\vartheta_2}{(1-\varepsilon_\phi))\vartheta_1}} = \sqrt{\frac{\lambda_2}{\lambda_1(1-\varepsilon_\phi)\varepsilon_p \lambda_{min}(Q)}}\frac{d_{max}}{\sqrt{k_{RB}}} \tag{47}$$

Remarks

1) The ultimate bound for the closed-loop dynamics in Eq. (28) is inversely proportional to the root-square of k_{RB}. For this reason, the control action (22) can be used to modulate the residual tracking error when the time goes to infinity. Hence, the

proposed extra control action provides robustness to the closed-loop system dynamics with respect to unmodelled dynamics and parameter uncertainties. It is shown in Section V (by numerical analysis) and in Section VI (by experiments) that this term plays a key role to reduce the residual tracking error of the gain-scheduling LQ strategy proposed in [13].

2) The tuning of the gain k_{RB} can be done by using Eq. (47) to provide an ultimate bound below a given threshold, say ρ_{lim}. It is noted that, for any choice of the LQ weights that satisfy (24) it is possible to find k_{RB} so that $\rho < \rho_{lim}$.
3) The control action u_{RB} linearly scales with k_{RB}. Consequently, according to [27], large k_{RB}values can negatively affect the closed-loop response during transients in terms of larger overshoots with respect to the reference trajectory and/or larger control actions. Hence, a trade-off between the residual error (28) and transient closed-loop dynamics should be adopted for the tuning of the k_{RB} gain.
4) Conditions (23)-(24) has been used in the analysis of closed-loop dynamics to compute an upper bound of the derivative of the Lyapunov function as shown Eq. (40). This upper bound is valid despite possible variations of the parameter-dependent matrix $P(v_x)$ which are generated the time varying nature of the vehicle speed and the gain-scheduling mechanism for the online adaptation the feedback gains (21) and (22). It is noted that, if $v_x(t)$ is known a priori (i.e. before the manoeuvre starts and for the entire manoeuvre), than it is possible to replace (23) with a Differential Riccati Equation (DRE) which has to be solved backward [16]. By using the DRE the time-varying nature of the matrix P is considered explicitly considered, thus condition (24) can be removed. However, the assumption of having the preliminary knowledge of $v_x(t)$ is restrictive as the longitudinal speed is decided by the driver. On the contrary, condition (24) can be easily verified a priori and, as shown in Section V, it is not restrictive as it might appear at first because it is always verified for common driving conditions (i.e. for a large range of longitudinal vehicle velocity and accelerations).
5) Assuming that the control input is bounded, i.e., $u \in [u_{min},\ u_{max}]$ is imposed for example by the actuation system, and that ΔA does not alter the asymptotic stability of the open-loop system (7), then the boundedness of the disturbance D in Eq. (31) can be guaranteed. Indeed, under these conditions, x remains bounded, as u and δ in Eq. (7) are bounded and the system is asymptotically stable, while the x_d is bounded as its first entry is fixed to zero and the second entry is the output of an asymptotically stable first order system. Notice that a similar analysis for assuring the boundedness of the disturbance acting on the vehicle dynamics has been carried out in [15].
6) Matching conditions of the form $D(t) = Bd(t)$, which imply that the D is in the direction of the input matrix B in (8),are often assumed in order to solve model reference control problems in presence of disturbances [28]–[30]. In Appendix B, it is shown that the direction of the disturbance D in (31) depends on a set of positive dimensionless functions, named as disturbance functions. These disturbance functions are denoted as $\tilde{d}_\beta$, $\tilde{d}_r$, $\tilde{d}_\delta$ and $\tilde{d}_{\delta m}$ and they are expressed as

$$\tilde{d}_\beta = \frac{\varphi_\beta}{\tilde{v}_x}, \quad \tilde{d}_r = \frac{\varphi_r}{\tilde{v}_x}, \quad \tilde{d}_\delta = \tilde{d}_{\delta p} + \tilde{d}_{\delta m}, \tag{48}$$

and

$$\tilde{d}_{\delta p} = \frac{\varphi_{\delta p}}{\tilde{v}_x}, \quad \tilde{d}_{\delta m} = \frac{\varphi_{\delta m}}{\tilde{v}_x}\left|\left(\frac{\tilde{C}_{\alpha r_0}\tilde{L}_b - \tilde{C}_{\alpha f_0}\tilde{L}_a}{\tilde{m}\tilde{v}_x^2} - 1\right)\frac{1}{\tilde{L}\left(1/\tilde{v}_x^2 + \tilde{k}_{us}\right)} - \tilde{C}_{\alpha f_0}\right|, \tag{49}$$

where $\tilde{v}_x$, $\tilde{C}_{\alpha f_0}$, $\tilde{C}_{\alpha r_0}$, $\tilde{L}_a$, $\tilde{L}_b$, $\tilde{m}$ and $\tilde{k}_{us}$ are the corresponding dimensionless values of quantities defined in Section II, and φ_β, φ_r, $\varphi_{\delta p}$ and $\varphi_{\delta m}$ are dimensionless coefficients (see Appendix B for further details). In Appendix B, it is shown that the disturbance is approximately in the direction of the input matrix when $\tilde{d}_\beta \ll 1$, $\tilde{d}_r \ll 1$, and $\tilde{d}_\delta \ll 1$. Moreover it is shown that the magnitude of $\tilde{d}_{\delta m}$ is a measurement of the mismatch between the system (7) with nominal parameters and the reference model (17) that cannot be compensated by the feed-forward control action (20), thus, when the condition $\tilde{d}_{\delta m} \ll 1$ holds then such mismatch can be neglected. Finally, it is remarked that, the disturbance functions scales as the inverse of the dimensionless longitudinal vehicle speed $\tilde{v}_x$. In Section V the disturbance functions in Eqs. (48) and (49) are studied and it is numerically showed that $\tilde{d}_\beta \ll 1$, $\tilde{d}_r \ll 1$, and $\tilde{d}_\delta \ll 1$ for all the simulated maneuvers.

A. Analytical comparison with the gain-scheduling LQR

Under the same assumptions made in Section III, this subsection analyses the closed-loop tracking error dynamics, when $u_{RB} = 0$ is applied to system (15). In other words, a control law with only the gain-scheduling LQR control action and the feedforward term is considered. The aim of this analysis is twofold, *(i)* to study from an analytical viewpoint how the control action u_{RB} in Eq. (22) modifies the closed-loop system dynamics, and *(ii)* to find for what values of the gain k_{RB}, the RLQR algorithm provides better performance with respect to the LQR strategy in terms of residual tracking error. Consequently, an analytical rule for the tuning of k_{RB} is provided. This analysis is performed as follow. First it is proven that when $u_{RB} = 0$, the tracking error is still globally uniformly ultimately bounded. Then the ultimate bound in this condition, denoted as ρ_{LQ}, is computed and compared to that provided by the RLQR, i.e., ρ in Eq. (28). Finally, values of k_{RB} such that $\rho < \rho_{LQ}$ are computed. Notice that this set of k_{RB}-values are those that allow improving the ultimate bound of the closed-loop system, and therefore, they can be used by practitioners for the design of u_{RB} (see Eq. (22)).

To prove the global uniform ultimate boundedness when $u_{RB} = 0$, the same steps in the previous section can be followed. Indeed, the tracking error dynamics are still described as in Eq. (31) with the only exception $\bar{u} = -u_{LQ}$. By selecting the Lyapunov function as in Eq. (35), inequalities (36) are still fulfilled. On the other hand, the derivative of the Lyapunov function computed along the solution of system (31) can be upper-bounded as follows:

$$\dot{V} \leq -\varepsilon_p \lambda_{min}(Q)\|e\|^2 + 2e^T PBd \leq -\varepsilon_p \lambda_{min}(Q)\|e\|^2 + 2\|e\|p_{max}d_{max} = -\widetilde{\Phi}_{LQ}(e) \tag{50}$$

with

$$p_{max} = \sup_{v_x \in [v_{xmin}, v_{xmax}]} \{\|P(v_x)B\|\}, \tag{51}$$

and

$$\widetilde{\Phi}_{LQ}(e) = \Phi_{LQ}(e) + (1-\varepsilon_\phi)\varepsilon_p \lambda_{min}(Q)\|e\|^2 - 2\|e\| p_{max} d_{max} \tag{52}$$

$$\Phi_{LQ}(e) = \varepsilon_\phi \varepsilon_p \lambda_{min}(Q)\|e\|^2, \quad \varepsilon_\phi \in (0,1). \tag{53}$$

When $\|e\| \geq \vartheta_{LQ}$, with

$$\vartheta_{LQ} = \frac{2 p_{max} d_{max}}{(1-\varepsilon_\phi)\varepsilon_p \lambda_{min}(Q)}, \tag{54}$$

then $(1-\varepsilon_\phi)\varepsilon_p \lambda_{min}(Q)\|e\|^2 - 2\|e\| p_{max} d_{max} \geq 0$, and therefore $-\widetilde{\Phi}_{LQ}(e) \leq -\Phi_{LQ}(e)$, which implies

$$\dot{V}(e) \leq -\Phi(e), \quad \forall \|e\| \geq \vartheta_{LQ}, \tag{55}$$

As confirmed in Eqs. (36) and (55), all the hypothesis required by Theorem 1 in Appendix A are fulfilled and therefore the tracking error system is globally uniformly ultimately bounded and the ultimate bound is

$$\rho_{LQ} = \sigma_1^{-1}\left(\sigma_2\left(\vartheta_{LQ}\right)\right) = \sqrt{\frac{\lambda_2}{\lambda_1}} \frac{2 p_{max}}{(1-\varepsilon_\phi)\varepsilon_p \lambda_{min}(Q)} d_{max}. \tag{56}$$

From the analysis, above, it is possible to point out that the control action u_{RB} in Eq. (22) can be used:

1) To enlarge the region of the state space where the closed-loop error trajectories are attracted toward the origin. Precisely, by choosing k_{RB} large enough, it is possible to have ϑ in Eq. (45) smaller than ϑ_{LQ} in Eq. (54). Consequently, the Lyapunov derivative is negative definite in a larger set of state space when RLQR is used.
2) To reduce the ultimate bound of the closed-loop system, or equivalently the residual tracking error. Indeed, by choosing k_{RB} large enough, ρ in Eq. (47) can be made smaller than ρ_{LQ} in Eq. (56). Therefore, it is possible to prove that,

$$\rho \leq \rho_{LQ} \Leftrightarrow k_{RB} \geq k_{RB}^{lim} \triangleq \frac{1}{4}\frac{(1-\varepsilon_\phi)\varepsilon_p \lambda_{min}(Q)}{p_{max}^2} \tag{57}$$

Remarks

1) The proof of the globally uniformly ultimately boundedness in the case of $u_{RB} = 0$ and the computation of the ultimate bound in Eq. (56) improve the result in [13] for the case vehicle dynamics are affected by disturbances and parameter uncertainties.
2) Compared to the gain-scheduling LQR, the RLQR introduces an additional degree-of-freedom, i.e., k_{RB}, which is shown to be fundamental to modulate the residual tracking error. In addition, Eq. (57) provides a tuning method for k_{RB} to reduce the

residual tracking error when the RLQR algorithm replaces the LQR strategy. This tracking error reduction will be extensively confirmed numerically and experimentally in Sections V and VI, respectively.

3) Despite the LQ control action makes the closed-loop system globally uniformly ultimately bound, the tuning of the LQ action to provide an ultimate bound below a given threshold, say ρ_{lim}, might not be trivial. The terms p_{max}, λ_1, and λ_2 in Eq. (56) depend on the LQ weights nonlinearly. Hence, LQ weighs so that $\rho_{LQ} < \rho_{lim}$ might not exist, thus time-consuming trial and error numerical procedures should be adopted to provide an adequate closed-loop ultimate bound.

V. Numerical Results

In this section, numerical results are analysed for a set of representative case studies to show the effectiveness of the proposed control method, by imposing required yaw rete references despite disturbances and parameter uncertainty. In addition, in order to confirm the superior performance achieved via the RLQR in terms of vehicle stability and handling, the closed-loop results are compared to those provided by a passive vehicle and an LQR controller with variable feedforward and feedback control gains proposed in [13] but not equipped with the additional control action (22) which characterizes the RLQR algorithm. To this aim, a quantitative comparison, by means of performance indexes, is carried out.

The numerical analysis is performed by using both MATLAB and IPG CarMaker integrated in one co-simulation tool. In IPG CarMaker an accurate model of an electric Range Rover Evoque with individually controlled motors on front and rear axles has been implemented. To ensure the validity of the results, the vehicle model also represents the characteristics of the vehicle used for experiments (see Section VI). Moreover, in the high-level control, the yaw rate feedback information is measured from IPG CarMaker, which mimics the yaw rate sensor in practice. The entire control system is instead developed in Matlab/Simulink. The middle level controller algorithm can be found in previous research [3].

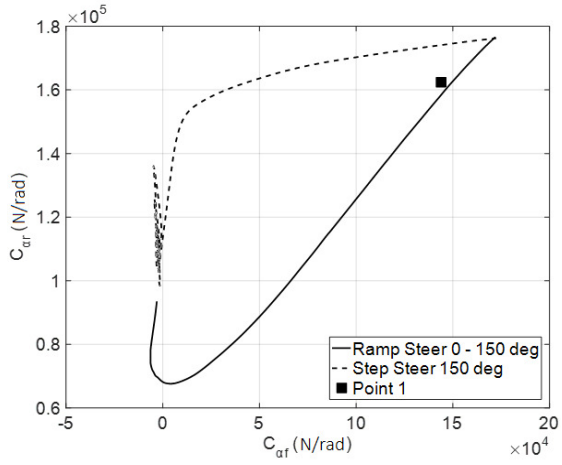

Figure 3. $C_{\alpha r}$ as function of $C_{\alpha f}$ during a ramp steer (continuous line) and a step steer (dashed line), and selected nominal values (Point 1)

Figure 3 represents the variations of the cornering stiffness during a ramp steer test and a step steer test. The nominal values for $C_{\alpha f_0}$ and $C_{\alpha r_0}$ are selected such that they are within the region limited by both manoeuvres, i.e., Point 1 in Figure 3. It is noted that the nominal values of the cornering stiffness correspond to the actual ones during manoeuvres requiring large lateral accelerations, thus reducing the magnitude of the disturbance due to parameter uncertainties during these more dangerous driving conditions. These two values were obtained through simulations with the IPG CarMaker model of the case study vehicle, including a Magic Formula tyre model with variable relaxation.

For control validation, two scenarios are considered where they are denoted as Test 1 and Test 2, respectively. For Test 1 the characteristics of cornering stiffness shown in Table 1 are used in IPG CarMaker and for the control design. Instead, in the case of Test 2, to further test the robustness of different control methods with respect to more severe parameter mismatches, the tyre model is changed in IPG CarMaker while the cornering stiffness values used for the control design are still those in Table 1.

TABLE 1 - VEHICLE PARAMETERS

Parameter	Value	Description
L_a	1.36 m	Front distance from CG
L_b	1.30 m	Rear distance from CG
$C_{\alpha f_0}$	$1.4 \cdot 10^5$ N/rad	Front cornering stiffness
$C_{\alpha r_0}$	$1.6 \cdot 10^5$ N/rad	Rear cornering stiffness
I_z	2761 kgm^2	Yaw moment of inertia
m	2025 kg	Vehicle mass

For each Test, three manoeuvres are carried out, namely: *(i)* sine-with-dwell, *(ii)* ramp steer, and *(iii)* step steer. The tracking performance provided by controllers are compared in terms of the resulting Root Mean Square Error (RMSE) value of the yaw rate during each manoeuvre, i.e.:

$$\mathrm{RMSE} = \sqrt{\frac{1}{t_f - t_i}\int_{t_i}^{t_f} (r_{ref}(t) - r(t))^2\, dt} \tag{58}$$

where t_f and t_i are the initial and final time instants of the steering input for the test, respectively. In addition, the control effort u is measured by computing the Integral of the Absolute value of the Control Action (IACA) during each manoeuvre as:

$$\mathrm{IACA} = \sqrt{\frac{1}{t_f - t_i}\int_{t_i}^{t_f} |u(t)|\, dt.} \tag{59}$$

Hence, RMSE and IACA represent the performance indexes to concisely evaluate quantitatively closed-loop performance.

The weights for the LQ controller have been chosen as $Q = \mathrm{diag}(1.5, \quad 80)$ and $R = 9 \cdot 10^{-10}$. Figure 4 shows the entries of the matrix $P(v_x)$ in (23) and those of the term $B^T P(v_x)$ which is used for the computation of the feedback gain-scheduling LQ and robust control actions in (21) and (22), respectively. Furthermore, as $B^T P(v_x)$ is bounded, the feedback control gains $K_{LQ}(v_x)$ and

$\overline{K}_{RB}(v_x)$ are bounded and converge to constant values for longitudinal vehicle speed larger than 80 km/h. Notice that in Figure 4a the entry P_{21} is not depicted as the solution of (23) is a symmetric matrix.

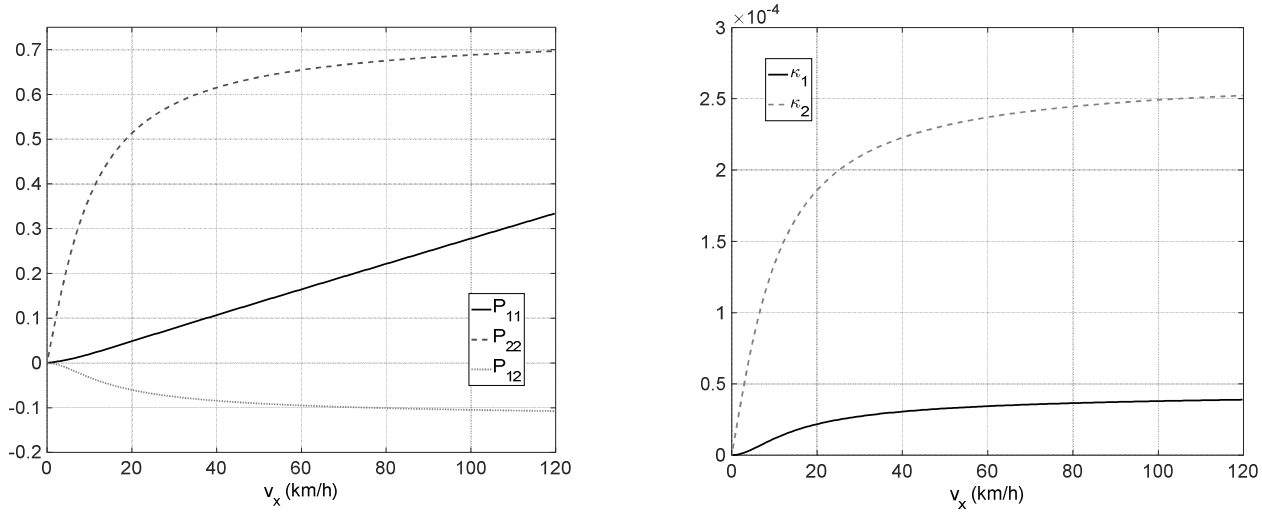

(a) (b)

Figure 4. a) Entries of the Riccati solution (23) and b) entries of the term $B^T P(v_x)$, with κ_1 and κ_2, being the first and second entry of $B^T P(v_x)$, respectively.

By defining $H = -\left(1-\varepsilon_p\right)Q - P(v_x)BR^{-1}B^T P(v_x) + a_x \frac{\partial P}{\partial v_x}(v_x)$, condition (24) is equivalent to require that the maximum eigenvalue of this matrix is negative[1], i.e.

$$\lambda_{max}(H) \leq 0\ ,\ \forall\ a_x\ \in\ [a_{xmin},\ a_{xmax}]. \tag{60}$$

It is noted that, as the $\partial P/\partial v_x$ is strictly positive definite for $v_x\ \in\ [0,\ 120]$ km/h (see Figure 5, where the $\lambda_{min}(\partial P/\partial v_x)$ is depicted), then negative longitudinal vehicle accelerations cannot change the sign of Eq. (60). On the other hand, for each speed v_x, there exists a maximum positive longitudinal vehicle acceleration a_x that changes the sign of Eq. (60). However, for each velocity $v_x\ \in\ [0,\ 120]$ km/h this critical acceleration is greater than 40 m/s^2, thus condition (60) is not restrictive for common driving conditions as it might appear at first. This is confirmed in Figure 6a where $\lambda_{max}(H)$ is depicted as a function of $v_x\ \in\ [0,\ 120]$ km/h and $a_x\ \in\ [-20,\ 40]$ m/s^2. Furthermore, for any v_x, $\lambda_{max}(H)$ increases for increasing positive a_x-values while decreases for negative decreasing a_x-values (see Figure 6b), thus confirming the aforementioned qualitative analysis.

[1] The matrixes $\partial P/\partial v_x$ and H are symmetric, thus their eigenvalues are real [31]. Consequently, the quantities $\lambda_{max}(H)$ and $\lambda_{min}(\partial P/\partial v_x)$ are well-posed.

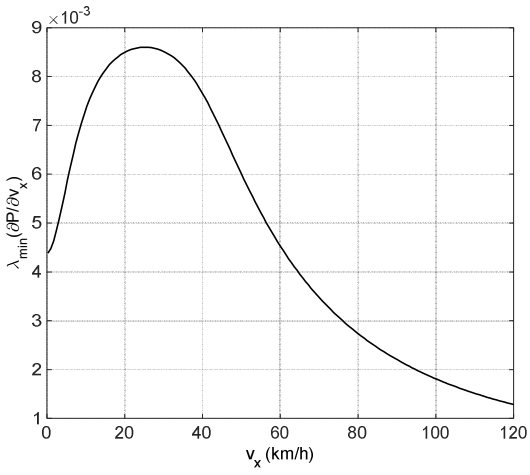

Figure 5. Minimum eigenvalue of the matrix $\partial P/\partial v_x$ as function of the vehicle speed.

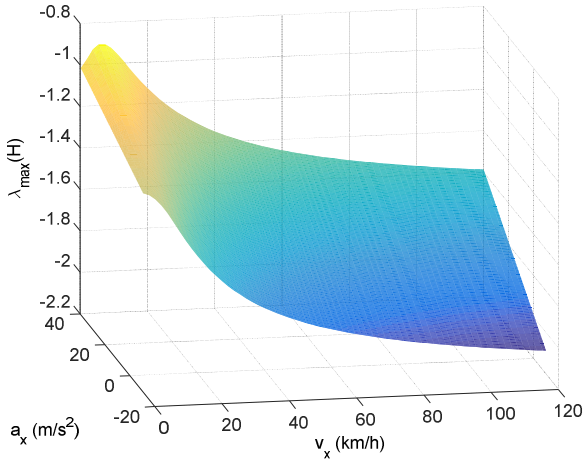

(a) (b)

Figure 6. a) $\lambda_{max}(H)$ as function of the longitudinal vehicle speed, v_x, and acceleration, a_x, and b) planar representation of the function $\lambda_{max}(H(v_x, a_x))$.

A. *Sine-with-Dwell*

It is obligatory that all commercial vehicles pass the sine with dwell test (FMVSS126) defined by the National Highway Traffic Safety Administration (NHTSA) in the United State to become road legal. For control validation, the sine with dwell test is used to verify the transient response of the vehicle. The manoeuvre consists of different stages with increasing steering wheel angle input. To validate the controller performance, only the most extreme manoeuvre is conducted since a vehicle passes all previous stages if the most extreme stage is passed. The simulation is set at $\delta_{sw} = 270$ deg at $v_x = 80$ km/h. The controller performance is measured through the maximum yaw rate at time 2.5s at which the yaw rate is required to be zero for the vehicle to pass the test. The yaw rate and sideslip responses of a passive vehicle, a vehicle controlled by LQR and a vehicle controlled by RLQR are plotted and compared in Figure 7a and Figure 7b. As the figures indicate, both LQR and RLQR demonstrate their capabilities to pass the test.

In Figure 7a, at time 0.8s, when the steering input returns to zero, the passive vehicle has lost its stability and failed the test. The RLQR controlled vehicle has followed the reference yaw rate closer with less overshoot compared to LQR controller.

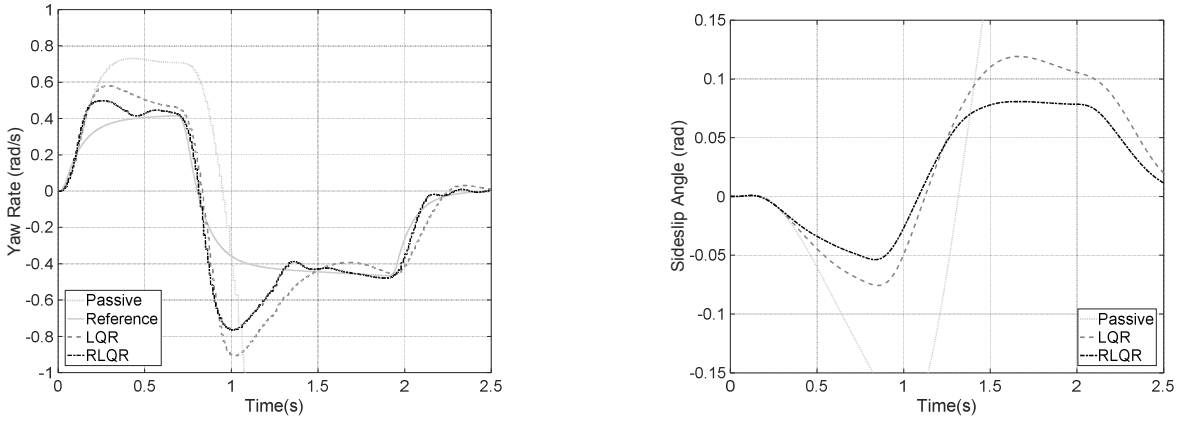

(a) (b)

Figure 7. Sine-with-dwell test simulation results. a) yaw rate comparison, b) side slip angle comparison.

Aa Figure 7b indicates, RLQR controller demonstrates a lower sideslip angle, which shows its capability to improve stability over the conventional LQR controller.

The yaw rate and sideslip responses of Test 2 are shown in Figure 8a and Figure 8b. The RLQR-controlled vehicle passes the sine-with-dwell test, while the LQR-controlled vehicle fails the test. The passive vehicle loses its stability and fails the test. The LQR lost track of the yaw rate reference from the beginning, representing the lack of robustness of LQR controller against parameter uncertainties.

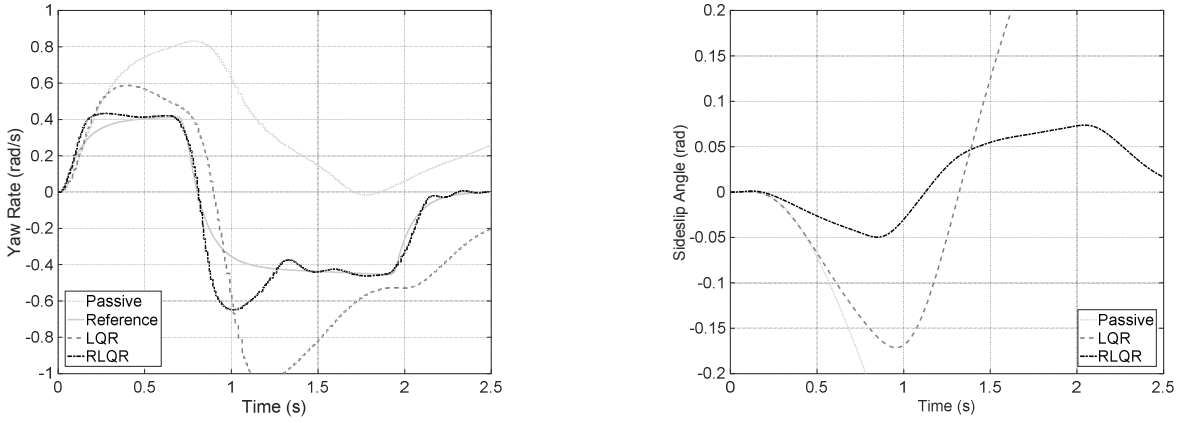

(a) (b)

Figure 8. Sine with dwell robustness test simulation results. a) yaw rate comparison, b) side slip angle comparison.

Table 2 shows the objective performance indicators calculated by the data obtained through simulations for both test cases. For Test 1, the RMSE values for the LQR controlled vehicle is within 18% of the passive vehicle, which is considerably lower than the passive vehicle. For the vehicle equipped with the RLQR controller, the RMSE value is within 9% of the passive vehicle and 50% improvement compared to the LQR controlled vehicle. The IACA values show that the control effort of the RLQR is slightly

higher than the LQR controlled vehicle. The LQR controlled vehicle has reduced the peak yaw rate error by 57% compared with the passive vehicle, whereas the RLQR has reduced the yaw rate error by 76% compared with the passive vehicle, and 44% compared to the LQR controlled vehicle. For the robustness test, the RMSE values for the RLQR controlled vehicle achieves 50% reduction over the LQR controlled vehicle. The IACA values show that the control effort of the RLQR is lower than the LQR controlled vehicle by 38%.

The LQR controlled vehicle has reduced the peak yaw rate error by 54% compared with the passive vehicle, whereas the RLQR has reduced the yaw rate error by 72% compared with the passive vehicle, and 38% compared to the LQR controlled vehicle.

TABLE 2 - OBJECTIVE PERFORMANCE INDICATORS FOR THE SINE-WITH-DWELL TESTS WITH DIFFERENT TYRES

	RMSE (rad/s)		IACA (Nm)		Peak Error (rad/s)	
	Test 1	Test 2	Test 1	Test 2	Test 1	Test 2
Passive	N/A	N/A	N/A	N/A	1.264	1.42
LQR	0.162	0.278	1361	2921	0.541	0.652
RLQR	0.082	0.112	1505	1824	0.305	0.405

B. Ramp Steer

The ramp steer test is used to investigate the robustness against unmodelled dynamics and parameter uncertainties. The understeering characteristics of the controlled vehicles are also investigated. In this test, the vehicle steering increases at a rate of $\dot{\delta}_{sw} = 10$ deg/s starting at $\delta_{sw} = 0$ deg at $v_x = 80$ km/h. Figure 9a shows the yaw rate comparison between the passive vehicle, LQR controlled vehicle and the RLQR controlled vehicle with nominal tyres. The vehicle controlled by RLQR has improved the steady state error of the yaw rate to zero, which shows that the controller is more robust against unmodelled dynamics of the system. It also can be seen that the transient state response of the RLQR has been improved.

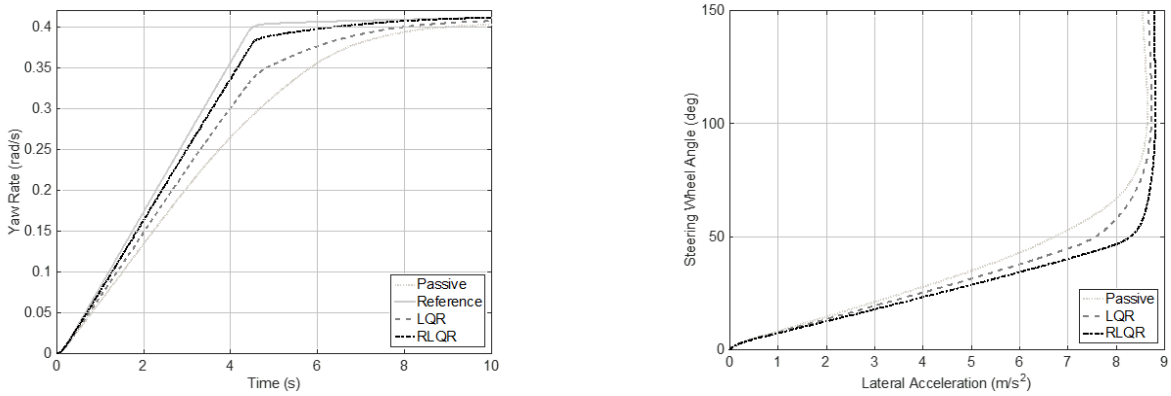

(a) (b)

Figure 9. Ramp steer test simulation results. a) yaw rate comparison, b) understeering characteristic comparison.

The RLQR closely tracks the reference, a 10% improvement over the conventional LQR controller during its transient state. As shown in Figure 9b, both RLQR and LQR controllers have increased the linear section of the steering wheel angle against lateral acceleration from 8.5 m/s^2. The RLQR has extended the maximum lateral acceleration to 8.8 m/s^2.

Figure 10 illustrates the ramp steer robustness test results. Figure 10a shows the RLQR proves its robustness against parameter uncertainties, as it closely tracks the reference yaw rate with zero steady state error. LQR during the robustness test does not reduce the steady state error. During the transient state, the performance of both LQR and RLQR is close to that of a standard ramp steer test. RLQR demonstrates its capability to extend the maximum lateral acceleration from 8 m/s^2 to 8.5 m/s^2 of the passive vehicle. Table 3 illustrates the objective performance indicators for the simulation results. The RMSE value for the proposed RLQR controller is within 43% of the passive vehicle and 50% of the LQR controlled vehicle. During the robustness test the RLQR is within 73% of the passive vehicle and 58% of the LQR controlled vehicle. This RMSE values suggest that the RLQR has a much superior tracking performance and its robustness against parameter uncertainties. The IACA values show that the RLQR utilises more control effort within a reasonable range to achieve better tracking performance and robustness. The RLQR controller has reduced the steady state error to near zero this is 90% and 88% better than the passive vehicle and the LQR controlled vehicle respectively. During the robustness test the RLQR has improved steady state tracking by 94% and 89% compared with passive and LQR controlled vehicle respectively, which is a significant improvement over the passive vehicle and the LQR controlled vehicle.

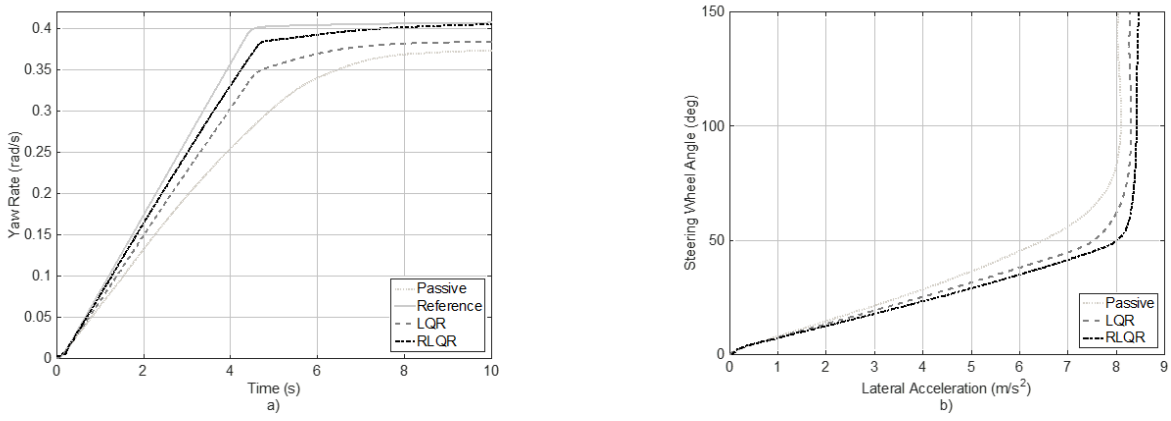

(a) (b)

Figure 10. Ramp steer robustness test simulation results a) yaw rate comparison, b) understeering characteristic comparison.

TABLE 3 - OBJECTIVE PERFORMANCE INDICATORS FOR RAMP STEER TESTS WITH DIFFERENT TYRES

	RMSE (rad/s)		IACA (Nm)		Peak Error (rad/s)	
	Test 1	Test 2	Test 1	Test 2	Test 1	Test 2
Passive	0.023	0.019	N/A	N/A	0.011	0.031
LQR	0.008	0.012	732	907	0.008	0.017
RLQR	0.004	0.005	1051	1541	0.001	0.002

C. Step Steer

The step steer test consists of a sharp steering with $\dot{\delta}_{sw} = 150$ deg/s at $v_x = 80$ km/h, verifying the controller performance during transient and steady states. As Figure 11 indicates, the passive vehicle significantly overshot the reference yaw rate. The LQR controlled vehicle has reduced the overshoot level by 16% with a steady state error. On the other hand, the RLQR reduced the overshoot by 32% and reduced the steady state error to near zero. The RLQR also improves the stability of the vehicle, as demonstrated by the sideslip angle.

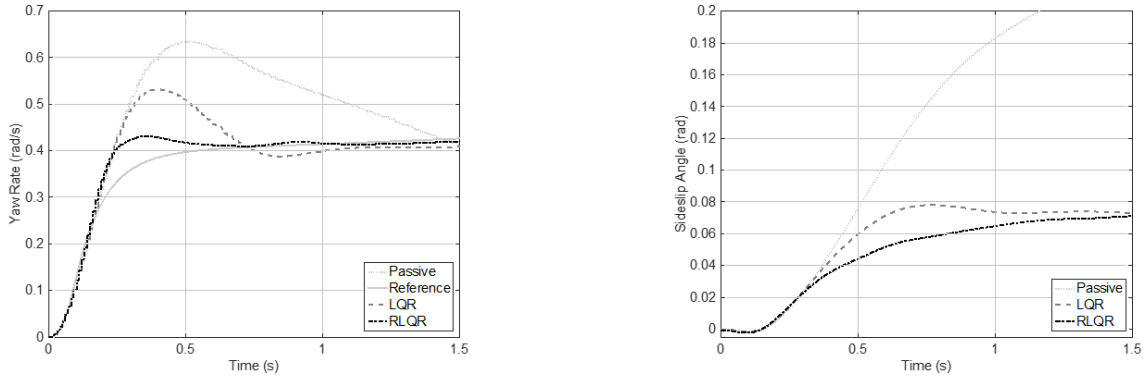

(a) (b)

Figure 11. Step steer test simulation results a) yaw rate comparison, b) understeering characteristic comparison

Figure 12 shows test result of the robustness test. In Figure 12a, the passive vehicle overshoot the reference yaw rate by 75%, where the LQR's performance degrades by 10% in terms of its peak overshoot. The RLQR demonstrated a similar result to the previous test during both transient and steady state periods. The sideslip angle of the RLQR controlled vehicle shows its robustness against parameter uncertainties. On the other hand, the LQR controlled vehicle shows 25% increase in sideslip angle at 0.6s.

Table 4 shows the objective performance indicators results for the tests. The RMSE of the RLQR controlled vehicle is within only 15% of the passive vehicle, whereas the LQR controlled vehicle is within 46%. This RMSE suggest that the RLQR has improved the tracking performance significantly over the LQR controller with 30% more control IACA value. These indicators also show that the peak yaw rate error for LQR and RLQR has been reduced by 38% and 72% respectively. For the robustness tests, the LQR is within 32% of the passive vehicle and the RLQR is within 13%. RLQR again shows significant improvement in tracking the reference yaw rate under both circumstances.

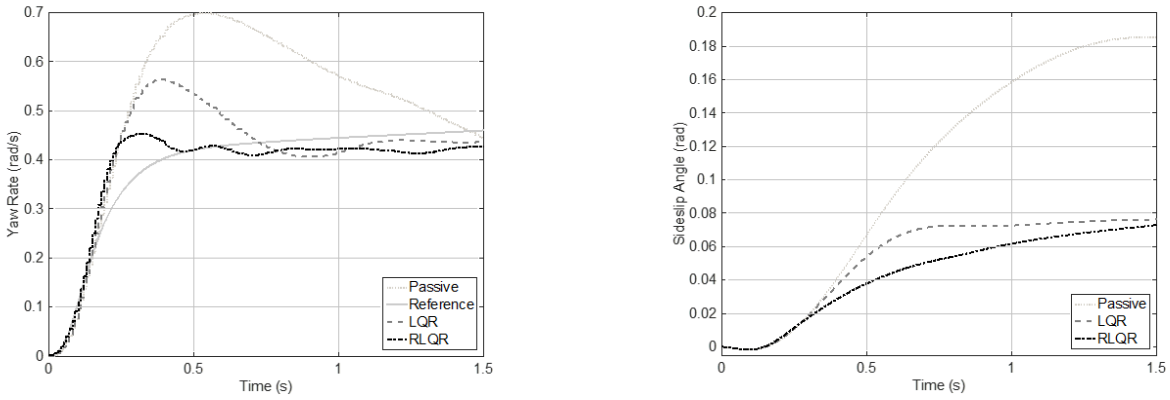

(a) (b)

Figure 12. Step steer robustness test simulation results. a) yaw rate comparison, b) understeering characteristic comparison

TABLE 4 - OBJECTIVE PERFORMANCE INDICATORS FOR STEP STEER TESTS WITH DIFFERENT TYRES

	RMSE (rad/s)		IACA (Nm)		Peak Error (rad/s)	
	Test 1	Test 2	Test 1	Test 2	Test 1	Test 2
Passive	0.052	0.076	N/A	N/A	0.234	0.295
LQR	0.024	0.025	102	105	0.145	0.182
RLQR	0.008	0.010	131	211	0.064	0.078

D. Numerical analysis of the disturbances

As an additional analysis of the closed-loop system dynamics, in this section the direction of the disturbance (33) for all the manoeuvres (i.e. sine with dwell, ramp steer and step steer) is numerically analysed through the use of the dimensionless disturbance functions $\tilde{d}_\beta$, $\tilde{d}_r$, $\tilde{d}_\delta$ and $\tilde{d}_{\delta m}$ defined in Appendix B. As shown in Appendix B, the disturbance term (33) is a linear combination of three dimensionless disturbance vectors, i.e. $\widetilde{D}_\beta$, $\widetilde{D}_r$ and $\widetilde{D}_\delta$ where the scalar coefficients of the linear combination are the dimensionless sideslip angle, yaw rate and steer angle, respectively. Consequently, if all the disturbance vectors are in the direction of the input matrix B in (8), then also the disturbance (33) is in that direction. In Appendix B is shown that a disturbance vector $\widetilde{D}_j$ is approximately in the direction of the input matrix if the corresponding disturbance function is such that $\tilde{d}_j \ll 1$, $j \in \{\beta, r, \delta\}$ as this function is the ratio between the components of $\widetilde{D}_j$ orthogonal and parallel to the B-matrix. Moreover, in Appendix B it is also shown that the magnitude of $\tilde{d}_{\delta m}$ is a measurement of the mismatch between the system (7) with nominal parameters and the reference model (17) that cannot be compensated by the feed-forward control action (20), thus when $\tilde{d}_{\delta m} \ll 1$ such mismatch can be neglected.

Table 5 shows for all the maneuvers examined in the previous sections three statistic indices (i.e. the mean value, the variance and the maximum value) for the disturbance functions. It is noted that the mean of the disturbance functions range from 0.009 to 0.0787, thus the component of the disturbance vectors parallel to the direction of the input matrix are, on the average, at least one

order of magnitude larger than the corresponding orthogonal component. Furthermore, also the maximum value for each disturbance function is smaller than one and never exceeds 0.15.

TABLE 5 – STATISTICS OF THE DISTURBANCE FUNCTIONS

	$\tilde{d}_\beta$			$\tilde{d}_r$			$\tilde{d}_\delta$			$\tilde{d}_{\delta m}$		
	Mean	Variance	Maximum	Mean	Variance	Maximum	Mean	Variance	Maximum	Mean	Variance	Maximum
Step Steer	0.0412	0.0003	0.0616	0.0149	0.0005	0.1310	0.0207	0.0007	0.1354	0.0198	0.0007	0.1346
Ramp Steer	0.0565	0.0012	0.1130	0.0220	0.0014	0.1366	0.0422	0.0017	0.1339	0.0414	0.0017	0.1331
Sin-with-Dwell	0.0787	0.0019	0.1450	0.0090	0.0002	0.1316	0.0168	0.0004	0.1355	0.0159	0.0004	0.1347

As the variance of the disturbance functions are small and their mean values never exceed 0.1, it is expected that most of the time the disturbance functions are below such a threshold. This is well confirmed by Table 6 which shows the percentage of the time the disturbance functions are below 0.1 with respect to the duration of the corresponding maneuver (i.e. $\Delta\tilde{T}_j(\%) = 100\Delta T_j / T$, where $j \in \{\beta, r, \delta, \delta_m\}$, and with ΔT_j being the time interval where $\tilde{d}_j < 0.1$ and T is the duration of the manoeuvre).

TABLE 6 – PERCENTAGE OF THE TIME WHERE THE DISTURBANCE FUNCTIONS ARE SMALLER THAN 0.1.

	$\Delta\tilde{T}_\beta(\%)$	$\Delta\tilde{T}_r(\%)$	$\Delta\tilde{T}_\delta(\%)$	$\Delta\tilde{T}_{\delta m}(\%)$
Step Steer	100	96.50	95.00	95.00
Ramp Steer	90.00	90.78	84.11	84.27
Sin-with-Dwell	68.05	98.60	98.09	98.09

The numerical analysis summarised in Table 5 and Table 6 confirms that for all the simulated maneuvers the component of the disturbance vectors orthogonal with respect to the input matrix can be neglected with respect to the parallel component, thus the disturbance vector is approximately in the direction of the B-matrix. Finally, for all the manoeuvres $\tilde{d}_\delta \approx \tilde{d}_{\delta m}$ (see the corresponding performance indices Table 5 and Table 6). Consequently, the first row of $\tilde{D}_\delta$ is mainly due to the mismatch between the system (7) with nominal parameters and the reference model (17) that cannot be compensated by the feed-forward action (20) (see also Appendix B where the analytical expression of $\tilde{D}_\delta$ is provided). However, as $\tilde{d}_{\delta m} \ll 1$, such mismatch can be neglected.

VI. EXPERIMENTAL RESULTS

For experimental validation of the proposed RLQR controller, a prototype 2011 electric Range Rover Evoque with individually controlled motors on front and rear axles is used. The experimental tests were performed at the Lommel proving ground in Belgium under dry road surface conditions during summer, a schematic and an exterior of the test vehicle can be found in Figure 13.

Figure 13. Electric vehicles with individually controlled motors during an experimental test and a schematic of the vehicle layout. M1, M2, M3 and M4: electric motors; I1, I2, I3 and I4: inverters: SCB: Slip Control Boost unit (electro-hydraulic braking system).

Skidpad test was conducted to validate the performance and robustness against unmodelled dynamics of the proposed controller. The skidpad test consists of the vehicle travel along a circular trajectory (30 m radius) at increasing speed up to $v_x = 80$ km/h. The steering wheel angle δ is progressively corrected by the test driver to follow the desired trajectory. This test validates the yaw rate tracking performance, robustness of the controller against unmodelled dynamics of the system and the understeering characteristic. Figure 14 shows the experimental yaw rate and the understeering characteristic of the vehicle. In Figure 14c, the proposed RLQR controller shows better tracking performance than the conventional LQR controller during the steady state. According to Figure 14d, the passive vehicle can only achieve 7 degs2/m, whereas LQR achieves 6.6 deg.s2/m and RLQR achieves 6 degs2/m. Both controlled vehicles can achieve more lateral acceleration from a smaller steering input which means that the controlled vehicle is more responsive than the uncontrolled vehicle. The RLQR also extends to the maximum lateral acceleration from 8.6 m/s2 (passive), 8.7 m/s2 (LQR) to 9.2 m/s2, meaning that the vehicle handling performance is enhanced and safety margin during emergency transient manoeuvres is increased [8]. The RLQR also demonstrated its tracking performance and its capacity in reducing steady state error. Table 7 demonstrates the performance improvement of the RLQR controller. The LQR controlled vehicle's yaw rate is within 44% of the passive vehicle, and the RLQR is within 66% of the passive vehicle.

The RLQR reduces the 22% of the RMSE value compared to the conventional LQR controller, while using only 16% more control effort. The RLQR also demonstrates better robustness against modelled uncertainties by reducing the steady state error by 60%, where LQR only reduces 40%.

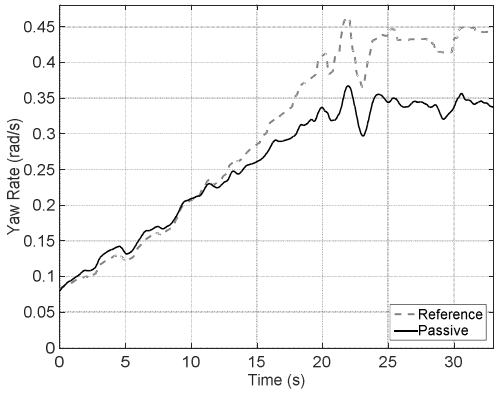

(a)

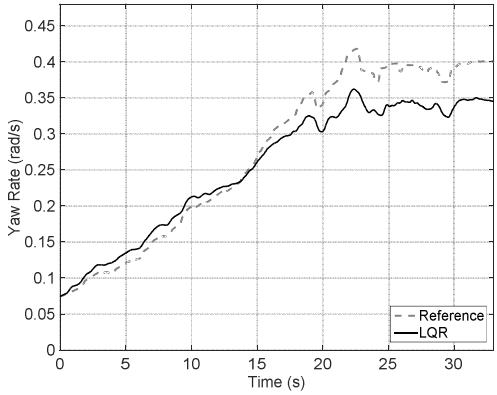

(b)

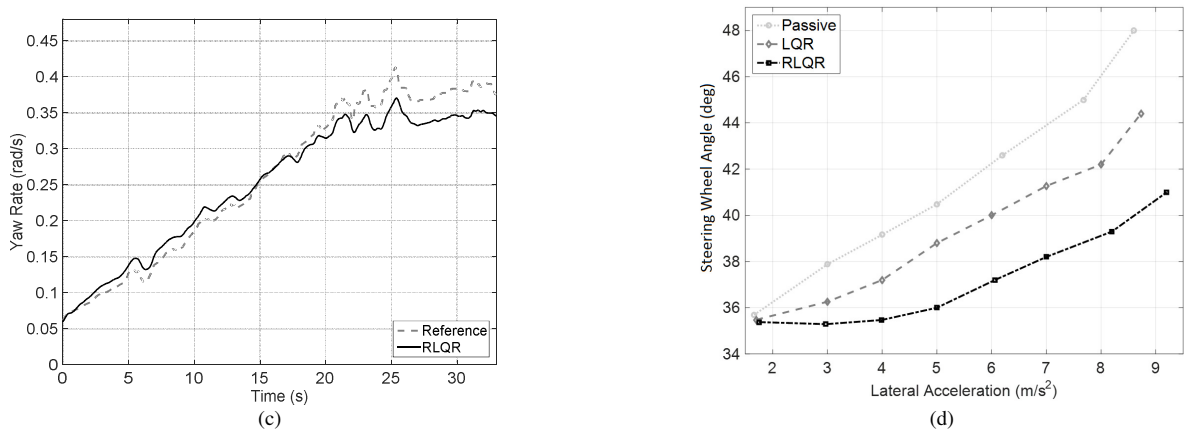

(c) (d)

Figure 14. Experimental skidpad test result comparison.

TABLE 7 - OBJECTIVE PERFORMANCE INDICATORS FOR SKIDPAD TESTS

	RMSE	IACA	Peak Error
Passive	0.068 rad/s	N/A	0.089 rad/s
LQR	0.038 rad/s	356 Nm	0.052 rad/s
RLQR	0.023 rad/s	413 Nm	0.037 rad/s

VII. CONCLUSION

This paper proposed a robust LQR controller, named RLQR, with variable gains to enhance both stability and handling performance of vehicle dynamics under system uncertainties and time-varying vehicle longitudinal velocity. The controller is composed of a feedforward action, an LQR feedback control action and a robust control action.

As the vehicle dynamics strongly depends on the vehicle longitudinal velocity, the control gains are scheduled as function of speed to adapt the close-loop system to speed variations. The RLQR augmented with the gain-scheduling mechanism was extensively validated numerically and experimentally. Both simulation and experimental results confirmed the superior performance of the RLQR with respect to a gain-scheduling LQR not equipped with the robust control action both in terms of reference yaw rate tracking and closed-loop robustness to parameter uncertainties, unmodelled dynamics, and disturbances. The effectiveness of the proposed control algorithm to tackle bounded disturbances was proven also analytically. Specifically, the analysis of the closed-loop system has shown that the RLQR guarantees that the tracking error is globally uniformly ultimately bounded. The bound is inversely proportional to the root-square of the gain of the additional control action. This explains the tracking error reduction when the RLQR algorithm replaces the LQR strategy. Future work will cover the experimental assessment of controller performance with different tyre characteristics, as well as low road friction conditions for additional robustness tests.

APPENDIX A

This appendix provides details about the theorem used in Section IV to derive the upper-bound of the closed-loop tracking error which is available in the technical literature of nonlinear system dynamics [22]. This theorem can be applied to nonlinear time-varying systems of the form

$$\dot{x} = f(t, x) \tag{61}$$

where $x \in \mathbb{R}^n$ is the state of the system, $f: \mathbb{R} \times \mathbb{R}^n \to \mathbb{R}^n$ is the system vector field, and n the dimension of the state-space, and it can be exploited to bound the system solutions when the time goes to infinity. Notice that, the notion used to formulate the next theorem are consistent with those used in [22].

Theorem 1 (Theorem 4.18 page 172 in [22]*).*

Let $D \subset \mathbb{R}^n$ be a domain that contains the origin and $V: [0, +\infty) \times D \to \mathbb{R}^n$ be a continuously differentiable function such that

$$\alpha_1(||x||) \leq V(t, x) \leq \alpha_2(||x||) \tag{62}$$

$$\dot{V}(t, x) = \frac{\partial V}{\partial t} + \frac{\partial V}{\partial x} f(t, x) \leq -W_3(x), \quad \forall \, \|x\| \geq \mu > 0. \tag{63}$$

$\forall \, t \geq t_0$ and $\forall \, x \in D \subset \mathbb{R}^n$, where α_1 and α_2 are class K functions and $W_3(x)$ is a continuous positive definite function. Take $r > 0$ such that $B_r \triangleq \{x \in \mathbb{R}^n : \big|||x|\big| \leq r\} \subset D$ *and suppose that*

$$\mu < \alpha_1^{-1}\big(\alpha_2(r)\big). \tag{64}$$

Then, there exists a class KL function $\beta: \mathbb{R}^+ \times \mathbb{R}^+ \to \mathbb{R}^+$ and for every initial state $x(t_0)$, satisfying $\|x(t_0)\| < \alpha_1^{-1}\big(\alpha_2(r)\big)$, there is $T \geq 0$ (dependent on $x(t_0)$ and μ) such that the solution of (61) satisfies

$$\|x(t)\| \leq \beta(\|x(t_0)\|, t - t_0) \quad \forall \, t \in [t_0, t_0 + T) \tag{65}$$

and

$$\|x(t)\| \leq \alpha_1^{-1}\big(\alpha_2(\mu)\big) \quad \forall \, t \in [\, t_0 + T, +\infty). \tag{66}$$

Moreover, if $D = \mathbb{R}^n$ and α_1 belongs to class K_∞, then (65) and (66) hold for any initial state $x(t_0)$, with no restriction on how large μ *is.* The reader is referred to [22] for its proof.

APPENDIX B

This appendix is devoted to the computation of the disturbance functions discussed in Section IV and their use to determine when the disturbance (33) is approximately in the direction of the input matrix B in (8), i.e. when the component of the disturbance

orthogonal to B can be neglected with respect to the component parallel to B. As the components of the disturbance orthogonal and parallel to the input matrix have different unit of dimensions, the first step for computing the dominant disturbance component is to make the dynamics of the error system (31) dimensionless, thus allowing to compare quantitatively the entries of the disturbance term. To this aim, the variables and parameters of system (31) are scaled as

$$\begin{gathered}\tilde{t} = t/\tau,\ \ \tilde{m} = m/M,\ \ \tilde{L} = L/l,\ \ \tilde{I}_z = I_z/i_z,\ \tilde{L}_a = L_a/l,\ \tilde{L}_b = L_b/l,\ \tilde{v}_x = v_x/V_x,\ \tilde{k}_{us} = k_{us}V_x^2,\\ \tilde{C}_{\alpha f_0} = C_{\alpha f_0}/C,\ \tilde{C}_{\alpha r_0} = C_{\alpha r_0}/C,\ \Delta\tilde{C}_{\alpha f} = \Delta C_{\alpha f}/C,\ \Delta\tilde{C}_{\alpha r} = \Delta C_{\alpha r}/C,\end{gathered} \tag{67}$$

where $\tau[\mathrm{s}]$, $M[kg]$, $l[m]$, $V_x[m/s]$, $i_z[kgm^2]$, and $C[N]$ are the scaling factors with suitable dimensions such that the quantities in (67) are dimensionless. By choosing τ as the largest time constant of the matrix $A_0(v_x)$ in (16) for a vehicle speed ranging for 5km/h to 120km/h, $l = L$ and $M = m$, as independent scaling factors and the remaining scaling factors as $V_x = l/\tau$, $i_z = Ml^2$, $C = Ml/\tau^2$, the dimensionless tracking error system is

$$\frac{d\tilde{e}}{d\tilde{t}} = \tilde{A}_0\tilde{e} + \tilde{B}\tilde{u} + \tilde{D} \tag{68}$$

where $\tilde{e}$, $\tilde{u}$, $\tilde{D}$ are the dimensionless tracking error, control input and disturbance, respectively, while the dimensionless input matrix $\tilde{B}$ and the dimensionless dynamic matrix $\tilde{A}_0$ have the same structure as those in Eqs. (8) and (16), respectively, i.e.,

$$\tilde{A}_0(\tilde{v}_x) = \begin{bmatrix} -\dfrac{\tilde{C}_{\alpha r_0} + \tilde{C}_{\alpha f_0}}{\tilde{m}\tilde{v}_x} & \dfrac{\tilde{C}_{\alpha r_0}\tilde{L}_b - \tilde{C}_{\alpha f_0}\tilde{L}_a}{\tilde{m}\tilde{v}_x^2} - 1 \\ \dfrac{\tilde{L}_b\tilde{C}_{\alpha r_0} - \tilde{L}_a\tilde{C}_{\alpha f_0}}{\tilde{I}_z} & -\dfrac{\tilde{L}_b^2\tilde{C}_{\alpha r_0} + \tilde{L}_a^2\tilde{C}_{\alpha f_0}}{\tilde{I}_z\tilde{v}_x} \end{bmatrix}, \quad \tilde{B} = \begin{bmatrix} 0 \\ \dfrac{1}{\tilde{I}_z} \end{bmatrix}, \tag{69}$$

but with parameters in Eq. (67).

After simple algebraic manipulations, it is possible to prove that the disturbance depends linearly on the dimensionless sideslip angle $\tilde{\beta}$, dimensionless vehicle yaw rate $\tilde{r}$, and dimensionless steering angle $\tilde{\delta}$, and it can be expressed as

$$\widetilde{D} = \widetilde{D}_\beta\tilde{\beta} + \widetilde{D}_r\tilde{r} + \widetilde{D}_\delta\tilde{\delta} \tag{70}$$

where the corresponding disturbance vectors $\widetilde{D}_\beta$, $\widetilde{D}_r$ and $\widetilde{D}_\delta$ are defined as

$$\begin{gathered}\widetilde{D}_\beta = \begin{bmatrix} \dfrac{\Delta\tilde{C}_{\alpha r} + \Delta\tilde{C}_{\alpha f}}{\tilde{m}\tilde{v}_x} \\ \dfrac{\tilde{L}_a\Delta\tilde{C}_{\alpha f} - \tilde{L}_b\Delta\tilde{C}_{\alpha r}}{\tilde{I}_z} \end{bmatrix}, \qquad \widetilde{D}_r = \begin{bmatrix} \dfrac{\tilde{L}_a\Delta\tilde{C}_{\alpha f} - \tilde{L}_b\Delta\tilde{C}_{\alpha r}}{\tilde{m}\tilde{v}_x^2} \\ \dfrac{\tilde{L}_b^2\Delta\tilde{C}_{\alpha r} + \tilde{L}_a^2\Delta\tilde{C}_{\alpha f}}{\tilde{I}_z\tilde{v}_x} \end{bmatrix}, \quad \widetilde{D}_\delta = \widetilde{D}_{\delta p} + \widetilde{D}_{\delta m}, \\ \widetilde{D}_{\delta p} = -\begin{bmatrix} \dfrac{\Delta\tilde{C}_{\alpha f}}{\tilde{m}\tilde{v}_x} \\ \dfrac{\tilde{L}_a\Delta\tilde{C}_{\alpha f}}{\tilde{I}_z} \end{bmatrix}, \quad \widetilde{D}_{\delta m} = -\begin{bmatrix} \left(\dfrac{\tilde{C}_{\alpha r_0}\tilde{L}_b - \tilde{C}_{\alpha f_0}\tilde{L}_a}{\tilde{m}\tilde{v}_x^2} - 1\right)\dfrac{\tilde{v}_x}{\tilde{L}\left(1 + \tilde{k}_{us}\tilde{v}_x^2\right)} + \dfrac{\tilde{C}_{\alpha f_0}}{\tilde{m}\tilde{v}_x} \\ 0 \end{bmatrix}.\end{gathered} \tag{71}$$

It is noted that $\widetilde{D}_\beta$, $\widetilde{D}_r$ and $\widetilde{D}_{\delta p}$ are the disturbance vectors generated by parameter uncertainties. Furthermore, the term $\widetilde{D}_{\delta m}$ is the disturbance vector due to mismatch between the system (7) with nominal parameters and the reference model (17) that cannot be

compensated by the feed-forward control action (20) and it is obtained under the assumption that the reference yaw rate is that provided by Eq. (9) and the dynamics of the filter (12) can be neglected with respect to the dynamics of the steering angle.

From (70), the disturbance $\widetilde{D}$ is approximately in the direction of the input matrix under the condition that each vector $\widetilde{D}_\beta$, $\widetilde{D}_r$ and $\widetilde{D}_\delta$ is approximately in the direction of the input matrix. From and engineering viewpoint, this condition can be guaranteed if for each disturbance vector the ratio between its component orthogonal and parallel to the direction of the input matrix is much smaller than one.

As the unit vectors orthogonal and parallel to the input matrix are $B_1^T = [1 \quad 0]$ and $B_2^T = [0 \quad 1]$, respectively, and considering that the component of a vector $\mathrm{Z} \in \mathbb{R}^2$ in the direction of B_j, $j = 1,2$, is $B_j^T \mathrm{Z}$, the aforementioned ratios are

$$\tilde{d}_\beta(\tilde{v}_x) \triangleq \frac{\left|B_1^T \widetilde{D}_\beta\right|}{\left|B_2^T \widetilde{D}_\beta\right|} = \frac{\varphi_\beta}{\tilde{v}_x}, \quad \varphi_\beta \triangleq \frac{\tilde{I}_z\left|\Delta\tilde{C}_{\alpha r} + \Delta\tilde{C}_{\alpha f}\right|}{\tilde{m}\left|\tilde{L}_a\Delta\tilde{C}_{\alpha f} - \tilde{L}_b\Delta\tilde{C}_{\alpha r}\right|}, \qquad \tilde{d}_r(\tilde{v}_x) \triangleq \frac{\left|B_1^T \widetilde{D}_r\right|}{\left|B_2^T \widetilde{D}_\beta\right|} = \frac{\varphi_r}{\tilde{v}_x}, \quad \varphi_r \triangleq \frac{\tilde{I}_z\left|\tilde{L}_a\Delta\tilde{C}_{\alpha f} - \tilde{L}_b\Delta\tilde{C}_{\alpha r}\right|}{\tilde{m}\left|\tilde{L}_b^2\Delta\tilde{C}_{\alpha r} + \tilde{L}_a^2\Delta\tilde{C}_{\alpha f}\right|}$$

$$\tilde{d}_\delta(\tilde{v}_x) \geq \frac{\left|B_1^T \widetilde{D}_\delta\right|}{\left|B_2^T \widetilde{D}_\delta\right|}, \quad \tilde{d}_\delta(\tilde{v}_x) \triangleq \tilde{d}_{\delta p}(\tilde{v}_x) + \tilde{d}_{\delta m}(\tilde{v}_x), \quad \tilde{d}_{\delta p}(\tilde{v}_x) \triangleq \frac{\varphi_{\delta p}}{\tilde{v}_x}, \quad \varphi_{\delta p} \triangleq \frac{\tilde{I}_z}{\tilde{m}\tilde{L}_a}, \tag{72}$$

$$\tilde{d}_{\delta m}(\tilde{v}_x) \triangleq \frac{\varphi_{\delta m}}{\tilde{v}_x}\left|\left(\frac{\tilde{C}_{\alpha r_0}\tilde{L}_b - \tilde{C}_{\alpha f_0}\tilde{L}_a}{\tilde{m}\tilde{v}_x^2} - 1\right)\frac{1}{\tilde{L}\left(1/\tilde{v}_x^2 + \tilde{k}_{us}\right)} - \tilde{C}_{\alpha f_0}\right|, \quad \varphi_{\delta p} \triangleq \frac{\tilde{I}_z}{\tilde{m}\tilde{L}_a} \quad \varphi_{\delta m} \triangleq \tilde{I}_z$$

where the dimensionless functions of the longitudinal speed, i.e. $\tilde{d}_\beta$, $\tilde{d}_r$, $\tilde{d}_\delta$, $\tilde{d}_{\delta p}$ and $\tilde{d}_{\delta m}$, are defined as disturbance functions. It is noted that from a geometric viewpoint the disturbance functions are also the absolute value of the sine of the angle between the corresponding disturbance vector and the input matrix.

Eqs. (72) implies that *(i)* the disturbance functions are inversely proportional to the vehicle longitudinal speed and *(ii)* the disturbance is in the direction of the input matrix with a good approximation when $\tilde{d}_\beta \ll 1$, $\tilde{d}_r \ll 1$, and $\tilde{d}_\delta \ll 1$. Furthermore, the disturbance function $\tilde{d}_{\delta m}$ is equal to $\left|B_1^T \widetilde{D}_{\delta m}\right| / \left|B_2^T \widetilde{D}_\delta\right|$, thus it is generated by the mismatch between the system (7) with nominal parameters and the reference model (17) that cannot be compensated by the feed-forward control action (20) proposed in [13]. When the condition $\tilde{d}_{\delta m} \ll 1$ holds this mismatch does not affect the direction of $\widetilde{D}$, thus it can be neglected. It is noted that the condition $\tilde{d}_{\delta m} \ll 1$ can be used as an alternative condition to that proposed in [13] for enabling the approximation of the equivalent input matrix to the plant input matrix (i.e. the approximation $B' \approx B$ in [13], page 1101, with B' being the equivalent input matrix) in the case the reference sideslip angle is set to zero and parameter variations are considered.

Notice that, in Section V it has been numerically proven that for all the simulated maneuvers the condition $\tilde{d}_\beta \ll 1$, $\tilde{d}_r \ll 1$, and $\tilde{d}_\delta \ll 1$ holds.

REFERENCES

[1] S. Fallah, A. Khajepour, B. Fidan, S.-K. Chen, and B. Litkouhi, "Vehicle optimal torque vectoring using state-derivative feedback and linear matrix inequality," *IEEE Transactions on Vehicular Technology*, vol. 62, no. 4, pp. 1540–1552, 2013.

[2] L. De Novellis, A. Sorniotti, P. Gruber, and A. Pennycott, "Comparison of feedback control techniques for torque-vectoring control of fully electric vehicles," *IEEE Transactions on Vehicular Technology*, vol. 63, no. 8, pp. 3612–3623, 2014.

[3] T. Goggia *et al.*, "Integral sliding mode for the torque-vectoring control of fully electric vehicles: Theoretical design and experimental assessment," *IEEE Transactions on Vehicular Technology*, vol. 64, no. 5, pp. 1701–1715, 2015.

[4] Y. Liu, B. Zhou, and S. Fang, "Sliding mode control of PMSM based on a novel disturbance observer," in *2009 4th IEEE Conference on Industrial Electronics and Applications*, 2009, pp. 1990–1994.

[5] A. Khajepour, M. S. Fallah, and A. Goodarzi, *Electric and Hybrid Vehicles: Technologies, Modeling and Control-A Mechatronic Approach*. John Wiley & Sons, 2014.

[6] S. Anwar, "Generalized predictive control of yaw dynamics of a hybrid brake-by-wire equipped vehicle," *Mechatronics*, vol. 15, no. 9, pp. 1089–1108, 2005.

[7] L. Del Re, F. Allgöwer, L. Glielmo, C. Guardiola, and I. Kolmanovsky, *Automotive model predictive control: models, methods and applications*, vol. 402. Springer, 2010.

[8] Q. Lu *et al.*, "Enhancing vehicle cornering limit through sideslip and yaw rate control," *Mechanical Systems and Signal Processing*, vol. 75, pp. 455–472, 2016.

[9] V. I. Utkin, "Sliding mode control design principles and applications to electric drives," *IEEE transactions on industrial electronics*, vol. 40, no. 1, pp. 23–36, 1993.

[10] H. Du, N. Zhang, and G. Dong, "Stabilizing vehicle lateral dynamics with considerations of parameter uncertainties and control saturation through robust yaw control," *IEEE Transactions on Vehicular Technology*, vol. 59, no. 5, pp. 2593–2597, 2010.

[11] D. V. Thang Truong, M. Meywerk, and W. Tomaske, "Torque vectoring for rear axle using Adaptive Sliding Mode Control," *2013 International Conference on Control, Automation and Information Sciences, ICCAIS 2013*, pp. 328–333, 2013.

[12] M. Canale, L. Fagiano, A. Ferrara, and C. Vecchio, "Vehicle yaw control via second-order sliding-mode technique," *IEEE transactions on industrial electronics*, vol. 55, no. 11, pp. 3908–3916, 2008.

[13] L. Li, G. Jia, J. Chen, H. Zhu, D. Cao, and J. Song, "A novel vehicle dynamics stability control algorithm based on the hierarchical strategy with constrain of nonlinear tyre forces," *Vehicle System Dynamics*, vol. 53, no. 8, pp. 1093–1116, 2015.

[14] E. Esmailzadeh, A. Goodarzi, and G. R. Vossoughi, "Optimal yaw moment control law for improved vehicle handling," *Mechatronics*, vol. 13, no. 7, pp. 659–675, 2003.

[15] C. Hu, R. Wang, F. Yan, and N. Chen, "Output Constraint Control on Path Following of Four-Wheel Independently Actuated Autonomous Ground Vehicles," *IEEE Transactions on Vehicular Technology*, vol. 65, no. 6, pp. 4033–4043, 2016.

[16] B. D. O. Anderson and J. B. Moore, "Optimal Control: Linear Quadratic Methods." Dover Books on Engineering, 2007.

[17] E. Soroka and U. Shaked, "On the robustness of LQ regulators," *IEEE Transactions on Automatic Control*, vol. 29, pp. 664–665, 1984.

[18] B. Mashadi, M. Mahmoodi-K, A. H. Kakaee, and R. Hosseini, "Vehicle path following control in the presence of driver inputs," *Proceedings of the Institution of Mechanical Engineers, Part K: Journal of Multi-body Dynamics*, vol. 227, no. 2, pp. 115–132, 2013.

[19] R. Xu, "Optimal sliding mode control and stabilization of underactuated systems," The Ohio State University, 2007.

[20] X. Liu, Y. Wu, Y. Zhang, and S. Xiao, "A control method to make LQR robust: A planes cluster approaching mode," *International Journal of Control, Automation and Systems*, vol. 12, no. 2, pp. 302–308, 2014.

[21] V. I. Utkin, *Sliding Modes in Control and Optimization*. Springer, 1992.

[22] H. Khalil, *Nonlinear Systems*. Prentice Hall, 2002.

[23] J. Mohammadpour and C. W. Scherer, *Control of linear parameter varying systems with applications*. Springer, 2012.

[24] W. Leithead and D. Leith, "Survey of gain-scheduling analysis and design.," *International journal of control*, vol. 73, no. 11, pp. 1001–1025, 2000.

[25] B. Jager, P. Neugebauer, R. Kriesten, N. Parspour, and C. Gutenkunst, "Torque-vectoring stability control of a four wheel drive electric vehicle," *IEEE Intelligent Vehicles Symposium, Proceedings*, vol. 2015–Augus, no. Iv, pp. 1018–1023, 2015.

[26] Q. Lu, A. Sorniotti, P. Gruber, J. Theunissen, and J. De Smet, "H∞ loop shaping for the torque-vectoring control of electric vehicles: Theoretical design and experimental assessment," *Mechatronics*, vol. 35, no. Supplement C, pp. 32–43, 2016.

[27] G. F. Franklin and J. D. Powell, *Feedback Control of Dynamic Systems*. Prentice Hall, 2005.

[28] D. P. Stoten and S. P. Hodgson, "Passivity-based analysis of the decentralized and extended minimal control synthesis algorithms," *International Journal of Control*, vol. 69, no. 5, pp. 633–646, 1998.

[29] H. Benchoubane and D. P. Stoten, "The decentralized minimal controller synthesis algorithm," *International Journal of Control*, vol. 56, no. 4, pp. 967–983, 1992.

[30] Y. D. Landau, *Adaptive Control: The Model Reference Approach*. CRC Pres, 1979.

[31] R. A. Horn, *Matrix Analysis*, 2 edition. Cambridge University Press, 2012.